

MIN3P-THCm Code Enhancements for Reactive Transport Modelling in Low Permeability Media

NWMO-TR-2015-12

July 2015

**Mingliang Xie¹, Pejman Rasouli¹, K. Ulrich Mayer¹ and
Kerry T. B. MacQuarrie²**

¹Department of Earth, Ocean and Atmospheric Sciences, University of British Columbia

²Department of Civil Engineering, University of New Brunswick

nwmo

NUCLEAR WASTE
MANAGEMENT
ORGANIZATION

SOCIÉTÉ DE GESTION
DES DÉCHETS
NUCLÉAIRES



Nuclear Waste Management Organization
22 St. Clair Avenue East, 6th Floor
Toronto, Ontario
M4T 2S3
Canada

Tel: 416-934-9814
Web: www.nwmo.ca

MIN3P-THCm Code Enhancements for Reactive Transport Modelling in Low Permeability Media

NWMO-TR-2015-12

July 2015

Mingliang Xie¹, Pejman Rasouli¹, K. Ulrich Mayer¹ and Kerry T. B. MacQuarrie²

¹Department of Earth, Ocean and Atmospheric Sciences, University of British Columbia

²Department of Civil Engineering, University of New Brunswick

This report has been prepared under contract to NWMO. The report has been reviewed by NWMO, but the views and conclusions are those of the authors and do not necessarily represent those of the NWMO.

All copyright and intellectual property rights belong to NWMO.

Document History

Title:	MIN3P-THCm Code Enhancements for Reactive Transport Modelling in Low Permeability Media		
Report Number:	NWMO-TR-2015-12		
Revision:	R000	Date:	July 2015
¹ Department of Earth, Ocean and Atmospheric Sciences, University of British Columbia			
² Department of Civil Engineering, University of New Brunswick			
Authored by:	Mingliang Xie ¹ , Pejman Rasouli ¹		
Verified by:	Kerry T. B. MacQuarrie ²		
Approved by:	K. Ulrich Mayer ¹		
Nuclear Waste Management Organization			
Reviewed by:	Tammy Yang		
Accepted by:	Mark Jensen		

ABSTRACT

Title: MIN3P-THCm Code Enhancements for Reactive Transport Modelling in Low Permeability Media
Report No.: NWMO-TR-2015-12
Author(s): Mingliang Xie¹, Pejman Rasouli¹, K. Ulrich Mayer¹ and Kerry T. B. MacQuarrie²
Company: ¹Department of Earth, Ocean and Atmospheric Sciences, University of British Columbia
 ²Department of Civil Engineering, University of New Brunswick
Date: July 2015

Abstract

The reactive transport code MIN3P-THCm was enhanced by strengthening its simulation capabilities for geochemical processes in low permeability porous media in which transport is diffusion-controlled. Code enhancements include a multisite ion exchange (MIE) model, a multicomponent diffusion (MCD) model, and a hybrid multicomponent diffusion (hMCD) model. Simulation capabilities were further extended by implementing domain discretization in radial coordinates, in addition to standard Cartesian coordinates. The code enhancements are useful for simulating reactive transport in engineered barrier systems and in low permeability host rock considered for deep geological repositories. This report documents the theoretical background, the governing equations, and the numerical implementation for these new ion exchange and diffusion modules. In addition, relevant sections of the updated user guide are described and verification examples for evaluation of the simulation capabilities are provided.

TABLE OF CONTENTS

	<u>Page</u>
ABSTRACT	iii
1. INTRODUCTION	1
2. OBJECTIVES AND SCOPE	1
3. MODEL FORMULATION, DEVELOPMENT AND USER GUIDE	2
3.1 GOVERNING EQUATIONS FOR REACTIVE TRANSPORT	2
3.1.1 Multisite Ion Exchange.....	3
3.1.2 Multicomponent Diffusion	4
3.1.3 Hybrid Multicomponent Diffusion.....	6
3.1.4 Extension of MCD and hMCD Models for Radial or Cylindrical Coordinates	7
3.2 NUMERICAL IMPLEMENTATION AND SOLUTION STRATEGY.....	9
3.2.1 Implementation of Multisite Ion Exchange Model	9
3.2.2 Implementation of Multicomponent Diffusion Model	11
3.2.3 Implementation of Hybrid Multicomponent Diffusion Model	12
3.2.4 Implementation of MCD and hMCD Models in Radial and Cylindrical Coordinates	13
3.3 USER GUIDE	14
3.3.1 Multisite Ion Exchange (MIE) Model.....	14
3.3.2 Multicomponent Diffusion (MCD) Model.....	15
3.3.3 Hybrid Multicomponent Diffusion (hMCD) Model.....	15
3.3.4 Radial and Cylindrical Coordinates for MCD and hMCD Models	20
4. MODEL VERIFICATION.....	20
4.1 MULTISITE ION EXCHANGE.....	20
4.1.1 Problem Definition.....	20
4.1.2 Model Set Up	21
4.1.3 Parameters	22
4.1.4 Results.....	23
4.1.5 Data Location	26
4.2 MULTICOMPONENT DIFFUSION.....	26
4.2.1 Problem Definition.....	27
4.2.2 Model Setup.....	27
4.2.3 Parameters	27
4.2.4 Results.....	27
4.2.5 File Location	28
4.3 MULTICOMPONENT DIFFUSION IN RADIAL COORDINATES	28
4.3.1 Problem Definition.....	28
4.3.2 Model Setup.....	29
4.3.3 Results.....	29
4.3.4 File Location	29
4.4 HYBRID MULTICOMPONENT DIFFUSION IN RADIAL COORDINATES	30
4.4.1 Problem Definition.....	30
4.4.2 Model Setup.....	31
4.4.3 Selected Experimental Data.....	31
4.4.4 Parameters	33

4.4.5	Results.....	33
4.4.6	File Location	34
5.	CONCLUSIONS	35
ACKNOWLEDGEMENTS.....		35
REFERENCES		36

LIST OF TABLES

	<u>Page</u>
Table 1: Composition of Initial and Boundary Solutions.....	22
Table 2: Physical and Chemical Parameters for the Benchmark.....	22
Table 3: Ion Exchange Reactions Used in the Simulation	25
Table 4: Selected Model Parameters Used for the Simulation of Nitric Acid Diffusion in NaCl Solution	27
Table 5: Composition of the Synthetic OPA Pore Water Used in the DR-A Diffusion and Sorption Experiments - Phase I (Calculated Based on NAGRA (2012))	31
Table 6: Composition of the Initial OPA Pore Water Used in the Simulation of the DR-A Diffusion and Sorption Experiments - Phase I (Based on Van Loon et al. 2003).....	32
Table 7: Selected Measured Tracer Concentrations [mol L ⁻¹] during the DR-A In-situ Diffusion Experiment - Phase I (Calculated Based on NAGRA (2012)).....	32
Table 8: General Parameters for the Circulation Chamber, Filter, Gap and OPA	33
Table 9: Free Aqueous Phase Diffusion Coefficients (D ₀) (Lide 1994), Correction Factors.....	33

LIST OF FIGURES

	<u>Page</u>
Figure 1: Grid Block Concept in Cylindrical Coordinates	13
Figure 2: Initial Sorbed Species Concentration Profiles Simulated by MIN3P-THCm (Lines) and CrunchFlow (Symbols), Left Panel – Sorbed Species on Site –X, Right Panel- Sorbed Species on Site –Y	21
Figure 3: Comparison of Breakthrough Curves at the Outflow Boundary Calculated by MIN3P-THCm (Lines) and CrunchFlow (Symbols): (a) Total Concentrations of Components in the Aqueous Phase, (b) pH, (c) Concentrations of Sorbed Species on Site –X, (d) Concentrations of Sorbed Species on Site –Y.....	24
Figure 4: Comparison of Sorbed Species Concentration Profiles at 10 Hours Simulated by MIN3P-THCm (Lines) and CrunchFlow (Symbols), Left – Sorbed Species on site–X, Right - Sorbed Species on Site –Y	25
Figure 5: Comparison of Sorbed Species Concentration Profiles at 50 Hours Simulated by MIN3P-THCm (Lines) and CrunchFlow (Symbols), Left – Sorbed Species on Site –X, Right - Sorbed Species on Site –Y	26
Figure 6: Comparison of Simulated Concentration Profiles Obtained from MIN3P-THCm (Lines), CrunchFlow (Open Symbols) and PHREEQC (Filled Symbols) at 100 Days..	28
Figure 7: Comparison of Simulated Concentration Profiles Obtained from MIN3P-THCm (Lines) and CrunchFlow (Symbols) at 100 Days	30
Figure 8: Schematic Diagram of the Simulation Domain Representing the Experimental Set-up Including the Borehole (Radius= 3.1 cm) that Contains the Tracers in Solution, Filter (4 mm in Thickness), Gap (3 mm in Thickness), and OPA up to A Radius of 61.5 cm. A Radial Coordinate System Was Used for the Simulations.....	31
Figure 9: Comparison of Experimental (Symbols) and Simulated (Lines) Concentration Curves of Tracers ⁸⁵ Sr ²⁺ (a), I ⁻ and Br (b), and HTO (c); and the Concentration Profiles of Tracers at 189 Days (d)	34

1. INTRODUCTION

Reactive transport modelling is an essential tool for the analysis of coupled physical, chemical and biological processes in earth systems, and has had significant impact on many fields including the evaluation of contaminant migration and attenuation in the subsurface (Steefel et al. 2005). Due to the complexity of coupled reactive transport problems in earth science and a high level of diversity in terms of applications, a number of reactive transport codes are being actively developed including PHREEQC, HPx, PHT3D, OpenGeoSys (OGS), HYTEC, ORCHESTRA, TOUGHREACT, eSTOMP, HYDROGEOCHEM, CrunchFlow, MIN3P-THCm, and PFLOTRAN (Steefel et al. 2014).

MIN3P-THCm is a general purpose multicomponent reactive transport code for variably saturated porous media; it is characterized by a high degree of flexibility and is applicable to a wide range of hydrogeological and geochemical problems. MIN3P-THCm was developed on the basis of the MIN3P code (Mayer 1999; Mayer 2002) and further developments including MIN3P-D (Henderson et al. 2009) and MIN3P-NWMO (Bea et al. 2011). Chemical processes that can be simulated include homogeneous reactions in the aqueous phase, as well as a variety of heterogeneous reactions. The code can simulate groundwater flow, solute transport, and geochemical reactions under variable density conditions in non-isothermal systems. The code is also suitable for highly saline conditions, can account for fluid pressure changes due to surface loading, and includes atmospheric boundary conditions (Bea et al. 2011 and 2012). MIN3P-THCm was previously applied to assess long-term geochemical stability in geological formations, specifically to evaluate redox stability in crystalline rocks of the Canadian Shield (Spiessl et al. 2008), and to simulate flow and reactive transport in a hypothetical sedimentary basin subjected to a glaciation/deglaciation cycle (Bea et al. 2011 and 2015).

Recent MIN3P-THCm code enhancements were motivated by participation in two international collaborative projects with an emphasis on simulation of transport and geochemical processes in low permeability media: (i) the Äspö Task Force on Engineered Barriers - Chemistry (EBS TF-C) focused on the study of diffusion and attenuation processes in highly compacted bentonite through well-defined laboratory experiments; and (ii) the in-situ diffusion, retention and perturbation (DR-A) experiment that was carried out at the Mont Terri Underground Rock Laboratory to investigate diffusion-dominated reactive transport in a claystone formation (Opalinus Clay). This report documents the related code developments.

2. OBJECTIVES AND SCOPE

To increase the capabilities of MIN3P-THCm for reactive transport modelling in low permeability porous media, such as engineered barrier materials and host rocks for a DGR, several code enhancements have been implemented, including:

- Addition of a multisite ion exchange (MIE) model;
- Addition of a multicomponent diffusion (MCD) model to account for species-dependent diffusion coefficients and electrochemical migration;
- Addition of a hybrid multicomponent diffusion (hMCD) model to empirically account for species-dependent effective diffusion parameters due to processes such as anion exclusion and enhanced cation diffusion;

- Implementation of radial and cylindrical coordinates in the MCD and hMCD models to facilitate simulation of in-situ borehole diffusion experiments.

After each code modification, at least one benchmark was added to the benchmark simulation suite to verify the functionality of the new development and to demonstrate its usage. In addition, the new capabilities (i.e. MCD and MIE) of MIN3P-THCm were verified and tested through code intercomparison with other reactive transport codes, namely CrunchFlow (Steefel 2008) and/or PHREEQC (Parkhurst and Appelo 1999), or experimental data. All code development activities were consistent with the QA/QC (Quality Assurance/Quality Control) requirements for NWMO software development (i.e. according to Technical Computing Software Procedure, Nuclear Waste Management Organization Document Number NWMO-PROC-EN-0002, Rev. R002). The version of MIN3P-THCm that includes the above mentioned code enhancements is version v1.0.203.

3. MODEL FORMULATION, DEVELOPMENT AND USER GUIDE

The governing equations, with a focus on the new developments, are detailed below. For additional details on the general code capabilities of MIN3P-THCm, the reader is referred to Mayer et al. (2002), Henderson et al. (2009), and Bea et al. (2011).

3.1 GOVERNING EQUATIONS FOR REACTIVE TRANSPORT

Diffusion is commonly simulated as a part of the hydrodynamic dispersion term (Bear 1972; Mayer et al. 2002), with the diffusion coefficient and tortuosity of all species assumed to be identical. However, for clayey materials (e.g. compacted bentonite) mass transport can be affected by more complex phenomena such as anion exclusion, species-dependent diffusion, and interlayer/surface diffusion. To account for these processes, alternative and enhanced model formulations are required (Shackelford and Moore 2013). Different approaches have been reported in the literature to address the complex phenomena for reactive diffusion in dense clayey materials (Bourg et al. 2003; Steefel et al. 2005). Ion migration in clays is often affected by adsorption reactions, in particular for cations, and adsorption reactions are often not restricted to a single surface site. For example, the sorption of Cs, K and Rb on illite via ion exchange occurs on three different exchange sites with different apparent affinities (Bolt et al. 1963; Brouwer et al. 1983). A general Cs sorption model for illite based on three exchange sites was developed by Bradbury and Baeyens (2000) and successfully applied to describe Cs isotherms in four different argillaceous rocks (i.e. Boom Clay, Oxford Clay, Palfris Marl and Opalinus Clay). A multisite modelling approach for cation exchange processes on illite has been successfully applied in predicting Cs sorption under various conditions of pH and ionic strength (e.g., Zachara et al. 2002; Bradbury and Baeyens 2011). This model was able to represent the different sorption properties of the various exchange sites (e.g. planar and edge sites).

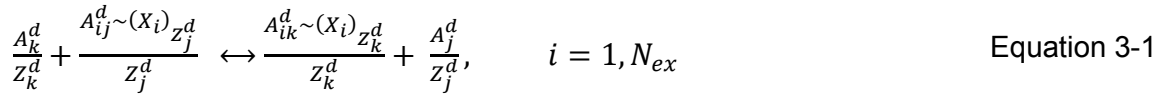
Giambalvo et al. (2002) applied a multicomponent diffusion model to simulate fluid-sediment interactions considering species dependent diffusion coefficients and electromigration to ensure maintenance of local charge balance. Furthermore, diffuse double layer (DDL) models based on the Donnan equilibrium assumption can handle the effect of surface charge in clay minerals on the migration of ions (Wersin et al. 2004; Appelo et al. 2008; Galindez et al. 2011). These

latter formulations include detailed descriptions of surface reactivity and/or of the mobility of interlayer species.

The following subsections focus on the theoretical background, numerical implementation in MIN3P-THCm, and introduce new sections for the MIN3P-THCm user guide related to the multisite ion exchange model, multicomponent diffusion model, and the hybrid multicomponent diffusion model.

3.1.1 Multisite Ion Exchange

Multicomponent cation exchange can be formulated using the Gaines-Thomas activity convention (Appelo and Postma 2003). Written in general form, cation exchange between the cations A_k^d and A_j^d and a multisite exchanger can be expressed as:



where Z_k^d and Z_j^d define the charge of the cations A_k^d and A_j^d in [meq mmol⁻¹], while $(Z_k^d)^{-1}$ and $(Z_j^d)^{-1}$ can be interpreted as the stoichiometric coefficients of the reaction equation. X_i is the i^{th} ion exchange site and N_{ex} is the number of exchange sites. To simplify the description, it is convenient to redefine the ion-exchange species as:

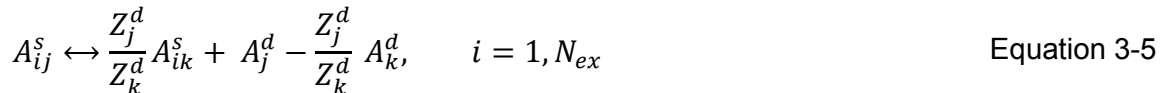
$$A_{ij}^s = A_{ij}^d \sim (X_i) Z_j^d \quad \text{Equation 3-2}$$

$$A_{ik}^s = A_{ik}^d \sim (X_i) Z_k^d \quad \text{Equation 3-3}$$

Substituting Equation 3-2 and Equation 3-3 into Equation 3-1 leads to:



Equation 3-4 can be rearranged to obtain a stoichiometric relationship with a unit stoichiometric coefficient for the cation exchange species A_{ij}^s :



The stoichiometric relationship in Equation 3-5 expresses cation exchange reactions in a general way involving any pair of dissolved cations on the ion exchange site X_i . This formulation has to be adjusted to facilitate its incorporation into the existing model equations. In this context, ion-exchange reactions are limited to exchange reactions involving cations, which are defined in the geochemical system as components. Equation 3-5 can be further generalized for any pair of ion-exchange reactions as:

$$A_{ij}^s \leftrightarrow v_{ij}^s A_{ik}^s + \sum_{l=1}^{N_c} v_{ijl}^s A_l^d, \quad i = 1, N_{ex}; j = 1, N_i^s \quad \text{Equation 3-6}$$

where v_{ij}^s is the stoichiometric coefficient of the ion-exchanged species A_{ik}^s in the j^{th} ion exchange reaction on the i^{th} ion exchange site, which is defined by the ratio of the charge of the two competing cations. N_c is the number of aqueous components. The parameters v_{ijl}^s are the stoichiometric coefficients of the components, in the j^{th} ion exchange reaction on the i^{th} ion exchange site. N_{ex} is the number of ion exchange sites, and N_i^s is the number of the ion-exchanged species on the i^{th} ion exchange site. The cations in dissolved form A_l^d can be expressed by the corresponding component concentration. However, because A_{ij}^s cannot be expressed exclusively in terms of aqueous components, but is dependent on the ion-exchanged species A_{ik}^s on each cation exchange site, one of the ion-exchanged species has to be chosen to represent A_{ik}^s . Based on the stoichiometry defined in Equation 3-6, the law of mass action can be applied to obtain a relationship that defines the fractions of the ion-exchanged species A_{ij}^s in terms of equivalent fractions:

$$\beta_{ij}^s = [K_{ij}^s]^{-1} [\beta_{ik}^s]^{v_{ij}^s} \prod_{l=1}^{N_c} (\gamma_l^c C_l^c)^{v_{ijl}^s}, \quad i = 1, N_{ex}; j = 1, N_i^s \quad \text{Equation 3-7}$$

where β_{ij}^s and β_{ik}^s are the fractions of the ion-exchanged species A_{ij}^s and A_{ik}^s on the i^{th} ion exchange site in [meq meq⁻¹] and K_{ij}^s refers to the selectivity coefficient for the j^{th} ion-exchange reaction on the i^{th} ion exchange site. γ_l^c is the activity coefficient of the l^{th} component as species in solution and C_l^c is the concentration of the l^{th} component as species in solution. Equation 3-7 only provides an explicit relationship for the calculation of β_{ij}^s if the fraction β_{ik}^s of the ion-exchanged species A_{ik}^s is known. It is not possible to determine β_{ik}^s using Equation 3-7. Therefore, an additional relationship is needed. This relationship can be defined as the sum of the fractions of all ion-exchanged species on the ion exchange site X_i , which equals 1 for each type of ion exchange site (Appelo and Postma 2003):

$$1 = \sum_{j=1}^{N_i^s} \beta_{ij}^s, \quad i = 1, N_{ex} \quad \text{Equation 3-8}$$

Equation 3-7 and Equation 3-8 constitute the set of equations defining the ion-exchange subproblem for the multisite ion exchange (MIE) model.

3.1.2 Multicomponent Diffusion

Working towards the goal to simulate complex ion migration phenomena in low permeability rock formations, a multicomponent diffusion (MCD) module was implemented in MIN3P-THCm (Rasouli 2015). The revised code enables the simulation of species-dependent diffusion and related electro-chemical migration processes (Rasouli 2015).

The general equation for diffusion-dominated reactive solute transport in fully saturated porous media can be expressed as:

$$\frac{\partial(\phi_e T_j^a)}{\partial t} + \frac{\partial T_j^s}{\partial t} + \nabla \cdot J_i^a = Q_j^{a,a} + Q_j^{a,m} + Q_j^{a,ext}, \quad j = 1, N_c \quad \text{Equation 3-9}$$

subject to the following definitions:

T_j^a total aqueous component concentration of the j^{th} component in [mol L⁻³ H₂O], defined as:

$$T_j^a = C_j^c + \sum_{i=1}^{N_x} v_{ij}^x C_i^x$$

T_j^s total concentration [mol L⁻³ porous medium] of the j^{th} aqueous component on the exchanger;

$Q_j^{a,a}$ internal source and sink terms from intra-aqueous kinetic reactions [mol L⁻³ porous medium T⁻¹];

$Q_j^{a,m}$ source-sink term due to mineral dissolution/precipitation reactions [mol L⁻³ porous medium T⁻¹];

$Q_j^{a,ext}$ external source and sink term [mol L⁻³ porous medium T⁻¹];

C_j^c concentrations of the components as species in solution [mol L⁻³ H₂O];

C_i^x concentrations of complexed species in solution [mol L⁻³ H₂O];

v_{ij}^x stoichiometric coefficients of the j^{th} component in the i^{th} complexed species;

ϕ_e effective porosity [-];

N_x number of aqueous complexes;

N_c number of aqueous components;

J_j^a total diffusive flux of the j^{th} component [M L⁻³ T⁻¹], described by the extended Nernst-Planck equation (Giambalvo et al. 2002):

$$J_j^a = - \left[\begin{array}{l} \tau_e \phi_e (D_{0,j}^c \nabla C_j^c + \sum_i^{N_x} D_{0,i}^x v_{ij}^x \nabla C_i^x) - \\ T_j^\varepsilon \frac{\sum_l^{N_c} z_l (\tau_e \phi_e D_{0,l}^c \nabla C_l^c + \sum_i^{N_x} v_{li}^x \tau_e \phi_e D_{0,i}^x \nabla C_i^x)}{\sum_k^{N_c} z_k T_k^\varepsilon} \end{array} \right] \quad \text{Equation 3-10}$$

where:

$D_{0,j}^c$ free diffusion coefficient of the j^{th} component as species in solution [L² T⁻¹];

$D_{0,i}^x$ free diffusion coefficient of the i^{th} complexed species in solution [L² T⁻¹];

ϕ_e effective porosity [-];

τ_e effective tortuosity [-];
 z_j charge number [-].

The variables T_j^ε (equally applicable for index k) in Equation 3-10 are defined as (Giambalvo et al. 2002):

$$T_j^\varepsilon = \tau_e \phi_e D_{0,j}^c z_j C_j^c + \sum_{i=1}^{N_x} \tau_e \phi_e D_{0,i}^x v_{ij}^x z_i C_i^x \quad \text{Equation 3-11}$$

The formulation outlined in Equation 3-9 through Equation 3-11 assumes that the effective porosity and the effective tortuosity are identical for all species.

3.1.3 Hybrid Multicomponent Diffusion

Further development of a hybrid multicomponent diffusion (hMCD) approach combines the multicomponent diffusion module with modified equations for species-dependent effective porosity and tortuosity. In essence, correction factors are introduced for the effective porosity and tortuosity for each individual species to capture the net effect of processes such as anion exclusion and interlayer/surface diffusion. While this is an empirical approach that requires calibration of the individual correction factors to experimental results, it does allow for the efficient simulation of several processes that may influence solute migration in low permeability, clay-rich media. Applying this approach consistently to Equation 3-9 through Equation 3-11 leads to:

$$\frac{\partial T_j^{\varepsilon,s}}{\partial t} + \frac{\partial T_j^s}{\partial t} + \nabla \cdot J_j^a = Q_j^{a,a} + Q_j^{a,m} + Q_j^{a,ext} \quad j = 1, N_c \quad \text{Equation 3-12}$$

with

$$T_j^{\varepsilon,s} = f_{\phi,j}^c \phi_e C_j^c + \sum_{i=1}^{N_x} f_{\phi,i}^x \phi_e v_{ij}^x C_i^x \quad \text{Equation 3-13}$$

$$J_j^a = - \left[\frac{\left(f_{\phi,j}^c \phi_e f_{\tau,j}^c \tau_e D_{0,j}^c \nabla C_j^c + \sum_{i=1}^{N_x} f_{\phi,i}^x \phi_e f_{\tau,i}^x \tau_e D_{0,i}^x v_{ij}^x \nabla C_i^x \right) - \sum_{l=1}^{N_c} z_l \left(f_{\phi,l}^c \phi_e f_{\tau,l}^c \tau_e D_{0,l}^c \nabla C_l^c + \sum_{i=1}^{N_x} f_{\phi,i}^x \phi_e f_{\tau,i}^x \tau_e D_{0,i}^x v_{li}^x \nabla C_i^x \right)}{T_j^{\varepsilon,d} \sum_{k=1}^{N_c} z_k T_k^{\varepsilon,d}} \right] \quad \text{Equation 3-14}$$

and

$$T_j^{\varepsilon,d} = f_{\tau,j}^c \tau_e f_{\phi,j}^c \phi_e D_{0,j}^c z_j C_j^c + \sum_{i=1}^{N_x} f_{\tau,i}^x \tau_e f_{\phi,i}^x \phi_e D_{0,i}^x v_{ij}^x z_i C_i^x \quad \text{Equation 3-15}$$

Equation 3-13 and Equation 3-15 are species-normalized total concentration terms for the mass storage term and diffusive transport term, respectively, accounting for species-dependent effective porosities, effective tortuosities, and free phase diffusion coefficients. Species-dependent effective tortuosities and porosities are expressed relative to a reference value using the correction factors $f_{\tau,j}^c$, $f_{\phi,j}^c$, $f_{\tau,i}^x$ and $f_{\phi,i}^x$, which are defined as:

- $f_{\tau,j}^c$ effective tortuosity correction factor for the j^{th} component as species in solution [-];
- $f_{\phi,j}^c$ effective porosity correction factor for the j^{th} component as species in solution [-];
- $f_{\tau,i}^x$ effective tortuosity correction factor for the i^{th} complexed species in solution [-];
- $f_{\phi,i}^x$ effective porosity correction factor for the i^{th} complexed species in solution [-].

3.1.4 Extension of MCD and hMCD Models for Radial or Cylindrical Coordinates

The above equations are expressed in general terms, and apply to a Cartesian coordinate system. For a two-dimensional cylindrical coordinate system the gradient terms in Equation 3-10 and Equation 3-14 must be replaced with the following terms (Istok 1989):

$$\nabla^2 C_i^c = \frac{\partial^2 C_i^c}{\partial r^2} + \frac{1}{r} \frac{\partial C_i^c}{\partial r} + \frac{\partial^2 C_i^c}{\partial z^2} = \frac{1}{r} \frac{\partial}{\partial r} \left(r \frac{\partial C_i^c}{\partial r} \right) + \frac{\partial^2 C_i^c}{\partial z^2} \quad \text{Equation 3-16}$$

$$\nabla^2 C_i^x = \frac{\partial^2 C_i^x}{\partial r^2} + \frac{1}{r} \frac{\partial C_i^x}{\partial r} + \frac{\partial^2 C_i^x}{\partial z^2} = \frac{1}{r} \frac{\partial}{\partial r} \left(r \frac{\partial C_i^x}{\partial r} \right) + \frac{\partial^2 C_i^x}{\partial z^2} \quad \text{Equation 3-17}$$

For a one-dimensional radial coordinate system, the gradient terms in Equation 3-10 and Equation 3-14 must be replaced with the following term:

$$\nabla^2 C_i^c = \frac{\partial^2 C_i^c}{\partial r^2} + \frac{1}{r} \frac{\partial C_i^c}{\partial r} = \frac{1}{r} \frac{\partial}{\partial r} \left(r \frac{\partial C_i^c}{\partial r} \right) \quad \text{Equation 3-18}$$

$$\nabla^2 C_i^x = \frac{\partial^2 C_i^x}{\partial r^2} + \frac{1}{r} \frac{\partial C_i^x}{\partial r} = \frac{1}{r} \frac{\partial}{\partial r} \left(r \frac{\partial C_i^x}{\partial r} \right) \quad \text{Equation 3-19}$$

in which r denotes position along the radial axis. For simplicity, only the MCD and hMCD models for radial coordinate systems are described below. Both models can be obtained in the same manner for cylindrical coordinates.

Combining Equation 3-10, Equation 3-18, and Equation 3-19, the diffusion term for the one-dimensional radial coordinate MCD model can be obtained:

$$\begin{aligned}
J_j^a &= - \left[\begin{array}{l} \tau_e \phi_e (D_{0,j}^c \nabla^2 C_j^c + \sum_i^{N_x} D_{0,i}^x v_{ij}^x \nabla^2 C_i^x) - \\ \sum_l^{N_c} z_l (\tau_e \phi_e D_{0,l}^c \nabla^2 C_l^c + \sum_i^{N_x} v_{li}^x \tau_e \phi_e D_{0,i}^x \nabla^2 C_i^x) \\ T_j^\varepsilon \frac{\sum_l^{N_c} z_l}{\sum_k^{N_c} z_k T_k^\varepsilon} \end{array} \right] \\
&= - \left\{ \begin{array}{l} \tau_e \phi_e \left[D_{0,j}^c \frac{1}{r} \frac{\partial}{\partial r} \left(r \frac{\partial C_j^c}{\partial r} \right) + \sum_i^{N_x} D_{0,i}^x v_{ij}^x \frac{1}{r} \frac{\partial}{\partial r} \left(r \frac{\partial C_i^x}{\partial r} \right) \right] - \\ T_j^\varepsilon \frac{\sum_l^{N_c} z_l \left[\tau_e \phi_e D_{0,l}^c \frac{1}{r} \frac{\partial}{\partial r} \left(r \frac{\partial C_l^c}{\partial r} \right) + \sum_i^{N_x} v_{li}^x \tau_e \phi_e D_{0,i}^x \frac{1}{r} \frac{\partial}{\partial r} \left(r \frac{\partial C_i^x}{\partial r} \right) \right]}{\sum_k^{N_c} z_k T_k^\varepsilon} \end{array} \right\}
\end{aligned} \tag{Equation 3-20}$$

All other terms remain the same as defined for the Cartesian coordinate system (Equation 3-9).

Similarly, combining Equation 3-14, Equation 3-18, and Equation 3-19, the diffusion term for the one-dimensional radial coordinate hMCD model can be obtained:

$$\begin{aligned}
J_j^a &= - \left[\begin{array}{l} (f_{\phi,j}^c \phi_e f_{\tau,j}^c \tau_e D_{0,j}^c \nabla^2 C_j^c + \sum_{i=1}^{N_x} f_{\phi,i}^x \phi_e f_{\tau,i}^x \tau_e D_{0,i}^x v_{ij}^x \nabla^2 C_i^x) - \\ \sum_{l=1}^{N_c} z_l (f_{\phi,l}^c \phi_e f_{\tau,l}^c \tau_e D_{0,l}^c \nabla^2 C_l^c + \sum_{i=1}^{N_x} f_{\phi,i}^x \phi_e f_{\tau,i}^x \tau_e D_{0,i}^x v_{li}^x \nabla^2 C_i^x) \\ T_j^{\varepsilon,d} \frac{\sum_{k=1}^{N_c} z_k T_k^{\varepsilon,d}}{\sum_{k=1}^{N_c} z_k T_k^{\varepsilon,d}} \end{array} \right] \\
&= - \left\{ \begin{array}{l} \left[f_{\phi,j}^c \phi_e f_{\tau,j}^c \tau_e D_{0,j}^c \frac{1}{r} \frac{\partial}{\partial r} \left(r \frac{\partial C_j^c}{\partial r} \right) + \sum_{i=1}^{N_x} f_{\phi,i}^x \phi_e f_{\tau,i}^x \tau_e D_{0,i}^x v_{ij}^x \frac{1}{r} \frac{\partial}{\partial r} \left(r \frac{\partial C_i^x}{\partial r} \right) \right] - \\ T_j^{\varepsilon,d} \frac{\sum_{l=1}^{N_c} z_l \left[f_{\phi,l}^c \phi_e f_{\tau,l}^c \tau_e D_{0,l}^c \frac{1}{r} \frac{\partial}{\partial r} \left(r \frac{\partial C_l^c}{\partial r} \right) + \sum_{i=1}^{N_x} f_{\phi,i}^x \phi_e f_{\tau,i}^x \tau_e D_{0,i}^x v_{li}^x \frac{1}{r} \frac{\partial}{\partial r} \left(r \frac{\partial C_i^x}{\partial r} \right) \right]}{\sum_{k=1}^{N_c} z_k T_k^{\varepsilon,d}} \end{array} \right\}
\end{aligned} \tag{Equation 3-21}$$

In a geochemical system dominated by primary species, effective porosity and tortuosity corrections for the secondary species can be neglected.

3.2 NUMERICAL IMPLEMENTATION AND SOLUTION STRATEGY

The governing equations for groundwater flow, heat transport, and reactive transport are implemented in MIN3P-THCm using a finite volume technique for spatial discretization and implicit time weighting for the temporal discretization. The reactive transport equations are solved using the global implicit approach, employing Newton's method for linearization (Mayer et al. 2002; Mayer and MacQuarrie 2010).

3.2.1 Implementation of Multisite Ion Exchange Model

In order to include ion-exchange reactions into the global mass conservation equations, three approaches are possible as described in Mayer (1999):

- Treatment of the ion-exchanged species A_{ij}^s as a component;
- Implicit solution of ion-exchange as a sub-problem;
- Explicit solution of ion-exchange as a sub-problem by derivation of an explicit relationship for the concentration calculation of the ion-exchanged species A_{ij}^s in terms of aqueous components.

If the ion-exchanged species A_{ij}^s is treated as a component, Equation 3-8 has to be included in the global system of mass conservation equations. In such cases, corresponding initial and boundary conditions for the ion-exchanged species A_{ij}^s are needed, which constitutes a quantity not generally available. It is therefore more convenient to treat ion-exchange reactions as a sub-problem that allows the treatment of all ion-exchanged species as secondary unknowns for the global problem. This can be achieved by substituting the equilibrium expression (Equation 3-7) for the ion-exchanged species A_{ij}^s into Equation 3-8:

$$1 = \sum_{j=1}^{N_i^s} [K_{ij}^s]^{-1} [\beta_{ik}^s]^{v_{ij}^s} \prod_{l=1}^{N_c} (\gamma_l^c C_l^c)^{v_{ijl}^s}, \quad i = 1, N_{es}; \quad j = 1, N_i^s \quad \text{Equation 3-22}$$

This equation contains the implicit solution for the fraction β_{ik}^s for the ion-exchanged species A_{ik}^s on the i^{th} exchange site. Once β_{ik}^s in Equation 3-22 is solved, the explicit solution of the fractions of all other ion-exchanged species can be obtained by Equation 3-7. However, an explicit solution cannot always be obtained owing to the nonlinearity of Equation 3-22 with respect to the fraction β_{ik}^s introduced by the stoichiometric coefficients v_{ij}^s defining the ratio of the charges of the ion-exchanged species pair. An implicit solution of the ion-exchange sub-problem is necessary if ion-exchange reactions involve trivalent or higher charged cations. However, Equation 3-22 can be simplified to a quadratic equation if only mono- and di-valent cations are participating in the ion-exchange reactions.

In such a case, an explicit solution can be obtained:

$$\beta_{ik}^s = \frac{-b + \sqrt{b^2 - 4ac}}{2a}, \quad i = 1, N_{es} \quad \text{Equation 3-23}$$

where the factors a , b and c are defined as:

$$a = \sum_{\substack{j=1 \\ v_{ij}^s=2}}^{N_i^s} [K_{ij}^s]^{-1} \prod_{l=1}^{N_c} (\gamma_l^c C_l^c)^{v_{ijl}^s}, \quad i = 1, N_{es}; j = 1, N_i^s \quad \text{Equation 3-24}$$

$$b = \sum_{\substack{j=1 \\ v_{ij}^s=1}}^{N_i^s} [K_{ij}^s]^{-1} \prod_{l=1}^{N_c} (\gamma_l^c C_l^c)^{v_{ijl}^s}, \quad i = 1, N_{es}; j = 1, N_i^s \quad \text{Equation 3-25}$$

$$c = -1 \quad \text{Equation 3-26}$$

The fractions of all other ion-exchanged species can be subsequently calculated according to Equation 3-7.

The actual concentration of the ion-exchanged species A_{ij}^s can be calculated by applying the conversion:

$$C_{ij}^s = \frac{\rho_b}{100} \alpha_i CEC (Z_j^s)^{-1} \beta_{ij}^s, \quad i = 1, N_{es}; j = 1, N_s \quad \text{Equation 3-27}$$

where C_{ij}^s is the concentration of the ion-exchanged species A_{ij}^s in [mol l⁻¹ bulk], ρ_b is the dry bulk density of the porous medium in [g cm⁻³ bulk], α_i is the fraction of the i^{th} ion exchange site and CEC is the total cation exchange capacity of the porous medium in [meq (100 g)⁻¹ solid]. The factor 100 provides the conversion factor in units of [g (100 g)⁻¹].

For the Gaines-Thomas activity convention it is assumed that each exchange site X_i has a charge of -1. For a single site ion exchange model, the cation exchange capacity (CEC) is equal to the sum of the charge equivalent concentrations of the adsorbed competing cations:

$$CEC = \sum_M Z_M q_M \quad \text{Equation 3-28}$$

in which Z_M and q_M are the charge and molar concentration of the sorbed cation M, respectively.

The formulation for the multisite cation exchange model is similar, but includes a summation over all exchange sites:

$$CEC = \sum_i \sum_M Z_M q_{(i)M} \quad \text{Equation 3-29}$$

where $q_{(i)M}$ is the molar concentration of the sorbed cation M on site type i .

3.2.2 Implementation of Multicomponent Diffusion Model

The governing equations (Equation 3-9 to Equation 3-11) for the MCD model have been implemented using the finite volume discretization method. Fully implicit time weighting is used for temporal discretization. For details on the discretized equations, the reader is referred to Mayer (1999):

$$\begin{aligned} & \frac{\phi_{e,k} V_k}{\Delta t} [T_{j,l}^{a,N+1} - T_{j,k}^{a,N}] + \frac{\phi_{e,k} V_k}{\Delta t} [T_{j,l}^{s,N+1} - T_{j,k}^{s,N}] - J_D + J_{EM} \\ & - Q_{j,k}^{a,a,N+1} V_k - Q_{j,k}^{a,m,N+1} V_k - Q_{j,k}^{a,ext,N+1} V_k = 0 \quad j = 1, N_c \end{aligned} \quad \text{Equation 3-30}$$

in which V_k and $\phi_{e,k}$ are the volume and the effective porosity of the k^{th} control volume, respectively. The notations N and $N+1$ stand for the previous and current time intervals. The term J_D refers to the molecular diffusion component of the multicomponent diffusion flux:

$$J_D = \sum_{l \in \eta_k} \frac{A_{kl}}{d_{kl}} \tau_{e,kl} \phi_{e,kl} \left[D_{0,j,kl}^c (C_{j,l}^{c,N+1} - C_{j,k}^{c,N+1}) + \sum_{i=1}^{N_x} D_{0,i,kl}^x v_{ij} (C_{i,l}^{x,N+1} - C_{i,k}^{x,N+1}) \right] \quad \text{Equation 3-31}$$

and J_{EM} refers to the electromigration component of the dispersion flux:

$$J_{EM} = \sum_{l \in \eta_k} \frac{A_{kl}}{d_{kl}} T_{j,kl}^{\varepsilon,N+1} \frac{\sum_{m=1}^{N_c} z_m \tau_{e,kl} \phi_{e,kl} \left[D_{0,m,kl}^c (C_{m,l}^{c,N+1} - C_{m,k}^{c,N+1}) + \sum_{i=1}^{N_x} D_{0,i,kl}^x v_{ij} (C_{i,l}^{x,N+1} - C_{i,k}^{x,N+1}) \right]}{\sum_{n=1}^{N_c} z_n T_{n,kl}^{\varepsilon,N+1}} \quad \text{Equation 3-32}$$

where z_m is the charge of the m^{th} aqueous component. The terms $T_{j,kl}^{\varepsilon,N+1}$ (equally valid for $T_{n,kl}^{\varepsilon,N+1}$) refer to:

$$T_{j,kl}^{\varepsilon,N+1} = \tau_{e,kl} \phi_{e,kl} \left[D_{0,j,kl}^c z_j C_{j,kl}^{c,N+1} + \sum_{i=1}^{N_x} D_{0,i,kl}^x v_{ij} z_i C_{i,kl}^{x,N+1} \right] \quad \text{Equation 3-33}$$

in which $C_{j,kl}^{c,N+1}$ is the representative concentration of the j^{th} component between control volumes k and l , and can be calculated based on the arithmetic mean:

$$C_{j,kl}^{c,N+1} = \frac{C_{j,k}^{c,N+1} + C_{j,l}^{c,N+1}}{2} \quad \text{Equation 3-34}$$

A_{kl} is the interfacial area between the control volumes k and l , and d_{kl} is the distance between the centroids of the control volumes. The material parameters (τ_e , ϕ_e and D_0) are defined on a control volume basis. It is therefore necessary to determine averaged values used for the calculation of interfacial fluxes. The default method is the distance-weighted harmonic mean. The representative values of effective porosity $\phi_{e,kl}$, effective tortuosity $\tau_{e,kl}$ and diffusion coefficient $D_{0,kl}$ can be calculated as:

$$\phi_{e,kl} = \frac{2\phi_{e,k}\phi_{e,l}d_{kl}}{\phi_{e,k}d_l + \phi_{e,l}d_k} \quad \text{Equation 3-35}$$

$$\tau_{e,kl} = \frac{2\tau_{e,k}\tau_{e,l}d_{kl}}{\tau_{e,k}d_l + \tau_{e,l}d_k} \quad \text{Equation 3-36}$$

$$D_{0,kl} = \frac{2D_{0,k}D_{0,l}d_{kl}}{D_{0,k}d_l + D_{0,l}d_k} \quad \text{Equation 3-37}$$

where d_k and d_l define the spatial extent of the two adjacent control volumes perpendicular to the interfacial area A_{kl} .

3.2.3 Implementation of Hybrid Multicomponent Diffusion Model

The governing equations (Equation 3-12 to Equation 3-15) for the hMCD model have been implemented on the basis of the MCD model:

$$\begin{aligned} M_j^{\varepsilon,s} + \frac{\phi_{e,k}V_k}{\Delta t}[T_{j,k}^{s,N+1} - T_{j,k}^{s,N}] - J_D + J_{EM} \\ - Q_{j,k}^{a,a,N+1}V_k - Q_{j,k}^{a,m,N+1}V_k - Q_{j,k}^{a,ext,N+1}V_k = 0 \quad j = 1, N_c \end{aligned} \quad \text{Equation 3-38}$$

in which the storage term $M_j^{\varepsilon,s}$ is:

$$M_j^{\varepsilon,s} = \frac{\phi_{e,k}V_k}{\Delta t}[f_{\phi,j}^c(C_{j,k}^{c,N+1} - C_{j,k}^{c,N}) + \sum_{i=1}^{N_x} f_{\phi,i}^x V_{ij}^x (C_{i,k}^{x,N+1} - C_{i,k}^{x,N})] \quad \text{Equation 3-39}$$

The term J_D refers to the molecular diffusion component of the dispersion flux:

$$J_D = \sum_{l \in \eta_k} \frac{A_{kl}}{d_{kl}} \tau_{e,kl} \phi_{e,kl} \left[f_{\phi,j}^c f_{\tau,j}^c D_{0,j,kl}^c (C_{j,l}^{c,N+1} - C_{j,k}^{c,N+1}) + \sum_{i=1}^{N_x} f_{\phi,i}^x f_{\tau,i}^x D_{0,i,kl}^x v_{ij} (C_{i,l}^{x,N+1} - C_{i,k}^{x,N+1}) \right] \quad \text{Equation 3-40}$$

and J_{EM} refers to the electromigration component of the dispersion flux:

$$J_{EM} = \sum_{l \in \eta_k} \frac{A_{kl}}{d_{kl}} T_{j,kl}^{\varepsilon,N+1} \frac{\sum_{m=1}^{N_c} z_m \tau_{e,kl} \phi_{e,kl} \left[f_{\phi,m}^c f_{\tau,m}^c D_{0,m,kl}^c (C_{m,l}^{c,N+1} - C_{m,k}^{c,N+1}) + \sum_{i=1}^{N_x} f_{\phi,i}^x f_{\tau,i}^x D_{0,i,kl}^x v_{ij} (C_{i,l}^{x,N+1} - C_{i,k}^{x,N+1}) \right]}{\sum_{n=1}^{N_c} z_n T_{n,kl}^{\varepsilon,N+1}} \quad \text{Equation 3-41}$$

where the terms $T_{j,kl}^{\varepsilon,N+1}$ (equally applicable for $T_{n,kl}^{\varepsilon,N+1}$) refer to:

$$T_{j,kl}^{\varepsilon,N+1} = \tau_{e,kl} \phi_{e,kl} \left[f_{\phi,j}^c f_{\tau,j}^c D_{0,j,kl}^c z_j C_{j,kl}^{c,N+1} + \sum_{i=1}^{N_x} f_{\phi,i}^x f_{\tau,i}^x D_{0,i,kl}^x v_{ij} z_i C_{i,kl}^{x,N+1} \right] \quad \text{Equation 3-42}$$

3.2.4 Implementation of MCD and hMCD Models in Radial and Cylindrical Coordinates

The implementations of the MCD and hMCD models in cylindrical coordinates are analogous to those in Cartesian coordinates. The difference lies in the grid block shape (Figure 1).

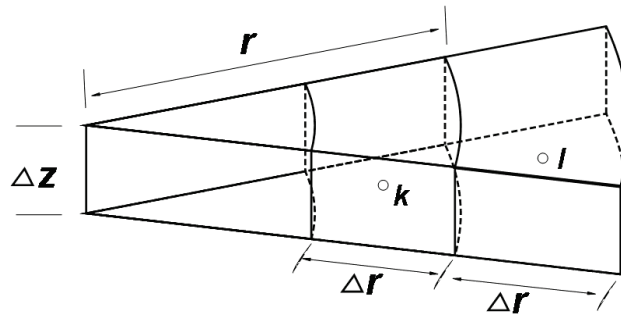


Figure 1: Grid Block Concept in Cylindrical Coordinates

The finite volume discretization method, which is equivalent to the block-centered finite difference method for cylindrical geometry, is applied. The interfacial areas and cell volumes for the radial grid are computed using the following formulas (Lapalla et al. 1987). The volume of the k^{th} control volume is calculated as:

$$V_k = [\pi r^2 - \pi(r - \Delta r)^2] \Delta z = 2\pi \Delta r \Delta z (r - \frac{\Delta r}{2}) \quad \text{Equation 3-43}$$

The interfacial area between k^{th} and l^{th} control volumes for the diffusive flux calculation along the radial coordinate can be calculated as:

$$A_{kl} = 2\pi r \Delta z \quad \text{Equation 3-44}$$

Finally, the interfacial area between k^{th} and l^{th} control volumes for the diffusive flux calculation perpendicular to the radial coordinate can be calculated as:

$$A_{kj} = \pi r^2 - \pi(r - \Delta r)^2 = 2\pi \Delta r (r - \frac{\Delta r}{2}) \quad \text{Equation 3-45}$$

3.3 USER GUIDE

3.3.1 Multisite Ion Exchange (MIE) Model

To apply this model, two keywords are needed in the MIN3P-THCm input file: 1) 'surface sites of ion-exchange' (in data block 2: geochemical system) - this keyword activates the model and is used to specify the number and names of all ion exchange sites; and 2) 'CEC fraction of multisite ion exchange' (in Data Block 14: initial condition - reactive transport) to specify the CEC fractions of each site. Below are two examples:

- a. Example for the keyword 'surface sites of ion-exchange'

```
'surface sites of ion-exchange'
3                               ; total number of ion exchange sites
'-FES'                         ; names of sites
'-II'
'-PS'
```

- b. Example for the keyword 'CEC fraction of multisite ion exchange'

```
'CEC fraction of multisite ion exchange'
0.0025                         ; '-FES'
0.20                            ; '-II'
0.7975                          ; '-PS'
```

In the example, three ion exchange sites are defined: site -FES with a fraction of 0.25 %, site -II with a fraction of 20 %, and site -PS with a fraction of 79.75 %.

It is important to note that the sum of the fractions of all sites should amount to 1.0. In addition, the name of each site should begin with '-'. The name of sorbed species should follow the site name plus (na). For example mg-PS(na) stands for the sorbed species of Mg²⁺ on the site -PS and exchanges with Na⁺. Ion exchange reactions are specified in the database file *sorption.dbs*. For example, the ion exchange reaction:



is specified in the database *sorption.dbs* as the following:

```
'mg-PS (na)'      0.0000  0.59          2.00  24.31200
 2  'mg+2'   1.000  'na+1' -2.000
```

Details on the parameters in the database can be found in the MIN3P-THCm user guide (Mayer et al. 2015).

3.3.2 Multicomponent Diffusion (MCD) Model

The MCD model can be activated by including the keyword 'multicomponent diffusion' in Data Block 1: global control parameters. If this option is activated, the free solution diffusion coefficients in water (D_0) for each primary and secondary species must be provided through the databases (i.e. in the file *comp.dbs* for primary species, in the file *complex.dbs* for secondary species).

Below is an example for the modified database entries (D_0 value highlighted in bold) in *comp.dbs*. Free phase diffusion coefficients must be included at the end of each entry in units of [$\text{m}^2 \text{s}^{-1}$]:

ca+2	2.0	6.00	.17	40.08000	.00	0.792d-9
cd+2	2.0	.00	.00	112.39940	.00	0.719d-9
cl-1	-1.0	3.00	.01	35.45300	.00	2.032d-9

This means that the D_0 of the primary species Ca^{2+} is $0.792 \times 10^{-9} \text{ m}^2 \text{ s}^{-1}$, D_0 of Cd^{2+} is $0.719 \times 10^{-9} \text{ m}^2 \text{ s}^{-1}$ and D_0 of Cl^- is $2.032 \times 10^{-9} \text{ m}^2 \text{ s}^{-1}$.

In addition, an example for entering the D_0 value (highlighted in bold) for secondary species in the database is shown below. The diffusion coefficients are included in *complex.dbs* at the end of the first line of each datablock:

oh-	13.3620	-13.9980	-1.00	3.50	.00	17.0074	1.00	5.273d-9
2	h2o			1.000	h+1		-1.000	

This means that the D_0 of the secondary species OH^- is $5.273 \times 10^{-9} \text{ m}^2 \text{ s}^{-1}$. Details on other parameters can be found in Mayer et al. (2015).

3.3.3 Hybrid Multicomponent Diffusion (hMCD) Model

The hMCD model can be activated by adding the keyword 'hybrid multicomponent diffusion' to Data Block 1: global control parameters. Then D_0 values for each primary and secondary species must be specified in the databases *comp.dbs* and *complex.dbs*, respectively, in the same way as described above for the MCD model. In addition, the correction factors for porosity and tortuosity for each primary and secondary aqueous species must be specified for each material group in the domain as follows:

- 1) The correction factors for effective porosity and tortuosity for each primary and secondary species may be provided for all material group(s) in Data Block 11: physical parameters - reactive transport. The user may specify correction factors for each material group separately. This feature is useful if the domain includes multiple material groups including for example sand and clay. In this case, correction factors are only needed for clay. If no correction factor data are provided for a material group, a default values of 1.0 will be applied, which means no modification of the effective porosity or tortuosity.
- 2) The correction factors for effective porosity of primary species are provided through the keyword 'porosity correction factor of primary species for hMCD diffusion' followed by the factors of each primary species in the same order as the components defined in Data Block 2: geochemical system under 'components'.
- 3) The correction factors for effective porosity of secondary species are provided through the keyword 'porosity correction factor of secondary species for hMCD diffusion' followed by the factors of each secondary species in the same order as the species defined in Data Block 2: geochemical system under 'secondary aqueous species'.
- 4) The correction factors for effective tortuosity of primary species are provided through the keyword 'tortuosity correction factor of primary species for hMCD diffusion' followed by the factors of each primary species in the same order as the components defined in Data Block 2: geochemical system under 'components'.
- 5) The correction factors for effective tortuosity of secondary species are provided through the keyword 'tortuosity correction factor of secondary species for hMCD diffusion' followed by the factors of each secondary species in the same order as the species defined in Data Block 2: geochemical system under 'secondary aqueous species'.

The following example shows the parameter setup for the hMCD model. The example domain includes four materials – a circulation chamber, a filter, an open water-filled gap, and a clay matrix ('background 1'). The hMCD model is applied only for the clay. The number of primary species is 17, while the number of secondary species is 23.

```
! Data Block 1: global control parameters
! -----
!
'global control parameters'
'Title: Task 2.2e_og Diffusion of Cs'
.true.                      ;varsat_flow
.true.                      ;steady_flow
.true.                      ;fully_saturated
.true.                      ;reactive_transport

'hybrid multicomponent diffusion'

'done'

! Data Block 2: geochemical system
! -----
!
'geochemical system'

'use new database format'

'database directory'
```

```

'.\database\MCDSr85'

'define input units'
'mol/l'

'components'
17 ;number of components (nc-1)
'cs+1' ; Cs
'na+1' ;component names
'k+1'
'mg+2'
'ca+2'
'sr+2'
'cl-1'
'h+1'
'o2(aq)'
'so4-2'
'co3-2'
'i-1'
'br-1'
'hto'
'co_60+2'
'eu+3'
'sr_85+2'

'secondary aqueous species'
23
'khso4(aq)'
'h2so4(aq)'
'oh-'
'mgoh+'
'mgco3aq'
'mghco3+'
'mgso4aq'
'caoh+'
'cahco3+'
'caco3aq'
'caso4aq'
'cahso4+'
'naco3-'
'nahco3aq'
'naso4-'
'kso4-'
'sroh+'
'hco3-'
'h2co3aq'
'hs04-'
'cscl(aq)'
'csi(aq)'
'csbr(aq)'

'linear sorption'
2
'sr_85+2'
'co_60+2'

'done'

! Data Block 11: physical parameters - reactive transport
!-----
!
```

```

'physical parameters - reactive transport'

!-----
'circulation chamber'

'longitudinal dispersivity'
0.0
'transverse horizontal dispersivity'
0.0
'transverse vertical dispersivity'
0.0
'end of zone'

!-----
!
'filter'
'longitudinal dispersivity'
0.0
'transverse horizontal dispersivity'
0.0
'transverse vertical dispersivity'
0.0
'end of zone'

!-----
!
'gap'
'longitudinal dispersivity'
0.0
'transverse horizontal dispersivity'
0.0
'transverse vertical dispersivity'
0.0
'end of zone'

!-----
!
'background 1' ; refers to clay rock
'longitudinal dispersivity'
0.0
'transverse horizontal dispersivity'
0.0
'transverse vertical dispersivity'
0.0

'porosity correction factor of primary species for hMCD diffusion'
1.0      ;'cs+'
1.0      ;'na+1'
1.0      ;'k+1'
1.0      ;'mg+2'
1.0      ;'ca+2'
1.0      ;'sr+2'
0.667   ;'cl-1'
1.0      ;'h+1'
1.0      ;'o2(aq)'
0.667   ;'so4-2'
0.667   ;'co3-1'
0.533   ;'i-1'
0.667   ;'br-1'
1.0      ;'HTO'
10.0    ;'co_60+2'
1.0      ;'eu+3'
3.5     ;'sr_85+2'

```

```

'tortuosity correction factor of primary species for hMCD diffusion'
 4.8      ;'cs+'
 1.0      ;'na+1'
 1.0      ;'k+1'
 1.0      ;'mg+2'
 1.0      ;'ca+2'
 1.0      ;'sr+2'
 0.55     ;'cl-1'
 1.0      ;'h+1'
 1.0      ;'o2(aq)'
 1.0      ;'so4-2'
 1.0      ;'co3-1'
 0.55     ;'i-1'
 0.38     ;'br-1'
 1.0      ;'HTO'
 3.0      ;'co_60+2'
 1.0      ;'eu+3'
 2.8      ;'sr_85+2'

'porosity correction factor of secondary species for hMCD diffusion'
 1.0      ;'khso4(aq)'
 1.0      ;'h2so4(aq)'
 1.0      ;'oh-'
 1.0      ;'mgoh+'
 1.0      ;'mgco3aq'
 1.0      ;'mghco3+'
 1.0      ;'mgso4aq'
 1.0      ;'caoh+'
 1.0      ;'cahco3+'
 1.0      ;'caco3aq'
 1.0      ;'caso4aq'
 1.0      ;'cahso4+'
 1.0      ;'naco3-'
 1.0      ;'nahco3aq'
 1.0      ;'naso4-'
 0.667    ;'kso4-'
 1.0      ;'sroh+'
 1.0      ;'hco3-'
 1.0      ;'h2co3aq'
 0.667    ;'hso4-'
 1.0      ;'cscl(aq)'
 1.0      ;'csi(aq)'
 1.0      ;'csbr(aq)'

'tortuosity correction factor of secondary species for hMCD diffusion'
 1.0      ;'khso4(aq)'
 1.0      ;'h2so4(aq)'
 0.55     ;'oh-'
 1.0      ;'mgoh+'
 1.0      ;'mgco3aq'
 1.0      ;'mghco3+'
 1.0      ;'mgso4aq'
 1.0      ;'caoh+'
 1.0      ;'cahco3+'
 1.0      ;'caco3aq'
 1.0      ;'caso4aq'
 1.0      ;'cahso4+'
 1.0      ;'naco3-'
 1.0      ;'nahco3aq'
 0.55     ;'naso4-'
 0.55     ;'kso4-'
 1.0      ;'sroh+'

```

```

0.55      ;'hco3-'
1.0       ;'h2co3aq'
0.55      ;'hso4-'
1.0       ;'cscl(aq)'
1.0       ;'csi(aq)'
1.0       ;'csbr(aq)'
'end of zone'

'done'

```

3.3.4 Radial and Cylindrical Coordinates for MCD and hMCD Models

To use the MCD and hMCD models in radial coordinates, the keyword 'radial coordinates' (highlighted in bold in example below) must be added in Data Block 3: spatial discretization. All other model input remains unchanged. Using this keyword, the x-coordinate of the Cartesian system is converted to the radial coordinate r. The y-coordinate is not used if the radial coordinate option is activated. If the z-coordinate is used, a cylindrical coordinate system is obtained. An example for a one-dimensional radial coordinate discretization is:

```

! Data Block 3: spatial discretization
! -----
!
'spatial discretization'
1                               ;number of discretization intervals in r
1000                            ;number of control volumes in interval r
0.0000E+00  0.1000E+04        ;rmin, rmax
1                               ;number of discretization intervals in y
1                               ;number of control volumes in interval
0. 1.0                          ;ymin,ymax
1                               ;number of discretization intervals in z
1                               ;number of control volumes in interval
0. 1.0                          ;zmin,zmax

'radial coordinates'

'done'

```

4. MODEL VERIFICATION

To verify the functionality of the new developments and to demonstrate their usage, at least one benchmark has been generated for each code enhancement, as described in the following subsections. The simulation results obtained with MIN3P-THCm are compared with the results simulated by CrunchFlow (Steefel 2008) and/or PHREEQC (Parkhurst and Appelo 1999) to facilitate verification by means of model intercomparison.

4.1 MULTISITE ION EXCHANGE

4.1.1 Problem Definition

This hypothetical benchmark is a multisite ion exchange problem with two material groups under steady state flow conditions. The MIN3P-THCm implementation was verified via code inter-comparison with CrunchFlow. CrunchFlow was previously applied for the simulation of Cs⁺ migration and retardation in the DI-A2 in-situ diffusion experiments in Opalinus Clay at the Mont

Terri Underground Rock Laboratory (Wersin et al. 2008) and to investigate Cs^+ release mechanisms at the Hanford site (Washington) (Zachara et al. 2002; Steefel et al. 2003; Chang et al. 2011). For all simulations using MIN3P-THCm and CrunchFlow, the Gaines-Thomas activity convention was applied.

4.1.2 Model Set Up

A one-dimensional, 16.0 m long domain was discretized into 101 control volumes, yielding a discretization interval of 0.16 m for the interior control volumes and 0.08 m for the control volumes on the boundaries. The domain contains two material groups: Material I (distributed from 0 to 8.0 m) and Material II (from 8.0+ to 16.0m). For simplicity, both materials have the same properties (i.e. hydraulic and transport parameters, CEC, and the same initial chemical composition of the pore water) except the CEC fractions of the two exchange site types (i.e. sites -X and -Y): the ion exchange site -X in Material I accounts for 90% of the total exchange sites, but only 40% for Material II (see Table 2 below).

Boundary conditions for the flow problem consist of a specified hydraulic head of 1.4 m on the left boundary and 0.0 m on the right boundary. The chemical compositions of the initial and boundary solutions are listed in Table 1. Initially, the pore water in the domain has elevated concentrations of Mg^{2+} , K^+ and Na^+ . The initial concentrations of the sorbed species on the ion exchange sites are calculated by assuming that the ion exchange sites are in equilibrium with the initial pore water. Consequently, the dominant initial sorbed species are Mg-X_2 , Na-X and K-X in Material I, and Mg-Y_2 and Na-Y in Material II (Figure 2). A low pH plume with elevated concentrations of Zn^{2+} , Pb^{2+} and Ca^{2+} and very low concentrations of Mg^{2+} , K^+ and Na^+ enters the domain from the left boundary via advective and diffusive transport, inducing fluid-rock interactions in the form of multisite ion exchange.

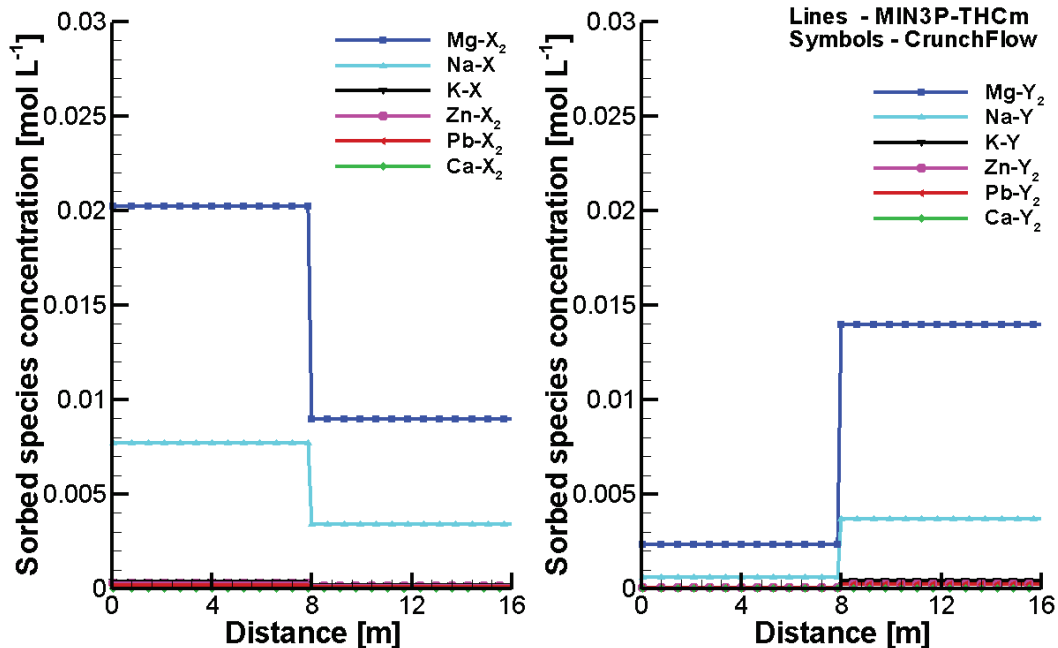


Figure 2: Initial Sorbed Species Concentration Profiles Simulated by MIN3P-THCm (Lines) and CrunchFlow (Symbols), Left Panel – Sorbed Species on Site -X, Right Panel- Sorbed Species on Site -Y

Table 1: Composition of Initial and Boundary Solutions

Parameter	Boundary solution	Initial solution	Unit
H ⁺	3.0	8.0	pH
^a SO ₄ ²⁻	3.645×10 ⁻³	5.147×10 ⁻⁴	[mol L ⁻¹]
Zn ²⁺	10 ⁻³	10 ⁻⁷	[mol L ⁻¹]
Pb ²⁺	10 ⁻³	10 ⁻⁷	[mol L ⁻¹]
Ca ²⁺	10 ⁻³	10 ⁻¹⁰	[mol L ⁻¹]
Mg ²⁺	10 ⁻¹⁰	10 ⁻⁵	[mol L ⁻¹]
K ⁺	10 ⁻¹⁰	10 ⁻⁵	[mol L ⁻¹]
Na ⁺	10 ⁻¹⁰	10 ⁻³	[mol L ⁻¹]

^aset to maintain charge balance

4.1.3 Parameters

The physical parameters (material properties) and the parameters for the multisite ion exchange reactions are summarized in Table 2.

Table 2: Physical and Chemical Parameters for the Benchmark

Parameter	Symbol	Value	Unit
Length of domain	<i>L</i>	16.0	[m]
Porosity	ϕ	0.25	[-]
Hydraulic conductivity	<i>K_{zz}</i>	1.0×10 ⁻³	[m s ⁻¹]
Free phase diffusion coefficient	<i>D₀</i>	1.0×10 ⁻⁹	[m ² s ⁻¹]
Longitudinal dispersivity	α_l	0.01	[m]
Soil bulk density	ρ_d	1.875	[g cm ⁻³]
Cation Exchange Capacity (CEC)	<i>CEC</i>	0.733	[meq (100g) ⁻¹ solid]
CEC fraction of site -X in material I	<i>F-X_I</i>	90%	[-]
CEC fraction of site -Y in material I	<i>F-Y_I</i>	10%	[-]
CEC fraction of site -X in material II	<i>F-X₂</i>	40%	[-]
CEC fraction of site -Y in material II	<i>F-Y₂</i>	60%	[-]

The ion exchange reactions for both sites ‘-X’ and ‘-Y’ are listed in Table 3. Exchange coefficients for the ‘-Y’ sites were assumed to be 50% larger than for the ‘-X’ sites, to provide a testing platform for the multi-site ion exchange model.

4.1.4 Results

Due to the ingress of groundwater from the left boundary with elevated concentrations of Zn^{2+} , Pb^{2+} and Ca^{2+} , and lower concentrations of Mg^{2+} , K^+ and Na^+ , the initial pore water in the domain is gradually replaced (Figure 3). After about 7 hours, the pH value at the right boundary begins to drop (Figure 3(b)) and after about 15 hours remains constant. The concentration of SO_4^{2-} begins to increase after about 7 hours. SO_4^{2-} reaches a maximum concentration $3.645 \times 10^{-3} \text{ mol L}^{-1}$, the same value as the concentration in the boundary solution, and remains constant thereafter. In contrast, the concentrations of the cations Na^+ , Mg^{2+} and K^+ begin to increase (Figure 3(a)). The maximum concentration of Na^+ reaches $5.2 \times 10^{-3} \text{ mol L}^{-1}$, higher than the concentration in the initial ($10^{-3} \text{ mol L}^{-1}$) and boundary ($10^{-10} \text{ mol L}^{-1}$) solutions, which is the result of displacement of the initially sorbed Na^+ ($Na\text{-X}$ and $Na\text{-Y}$) by Zn^{2+} , Pb^{2+} and Ca^{2+} (Figure 4, Figure 5). Similarly, the cations Mg^{2+} and K^+ show the same trend. The concentrations of sorbed species on both types of exchange sites change accordingly (depicted in Figure 4 at 10 hours and in Figure 5 at 50 hours). The results show a decrease of the concentrations of the initially dominant sorbed species $Mg\text{-X}_2$, $Mg\text{-Y}_2$, $Na\text{-X}$ and $Na\text{-Y}$, and an increase of $Zn\text{-X}_2$, $Zn\text{-Y}_2$, $Pb\text{-X}_2$, $Pb\text{-Y}_2$, $Ca\text{-X}_2$ and $Ca\text{-Y}_2$. $K\text{-X}$ and $K\text{-Y}$ behave similarly to $Na\text{-X}$ and $Na\text{-Y}$, but the concentrations are much lower.

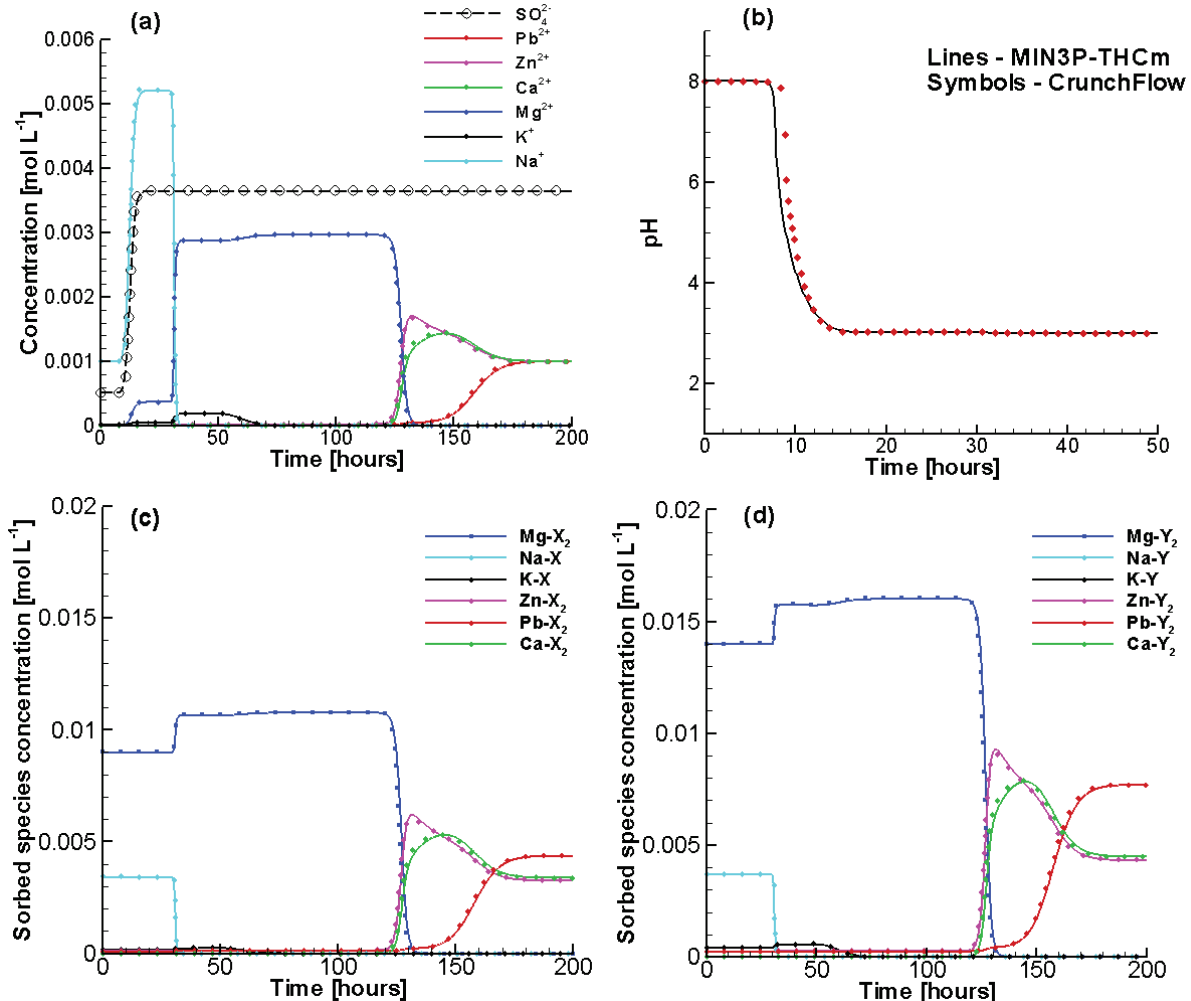
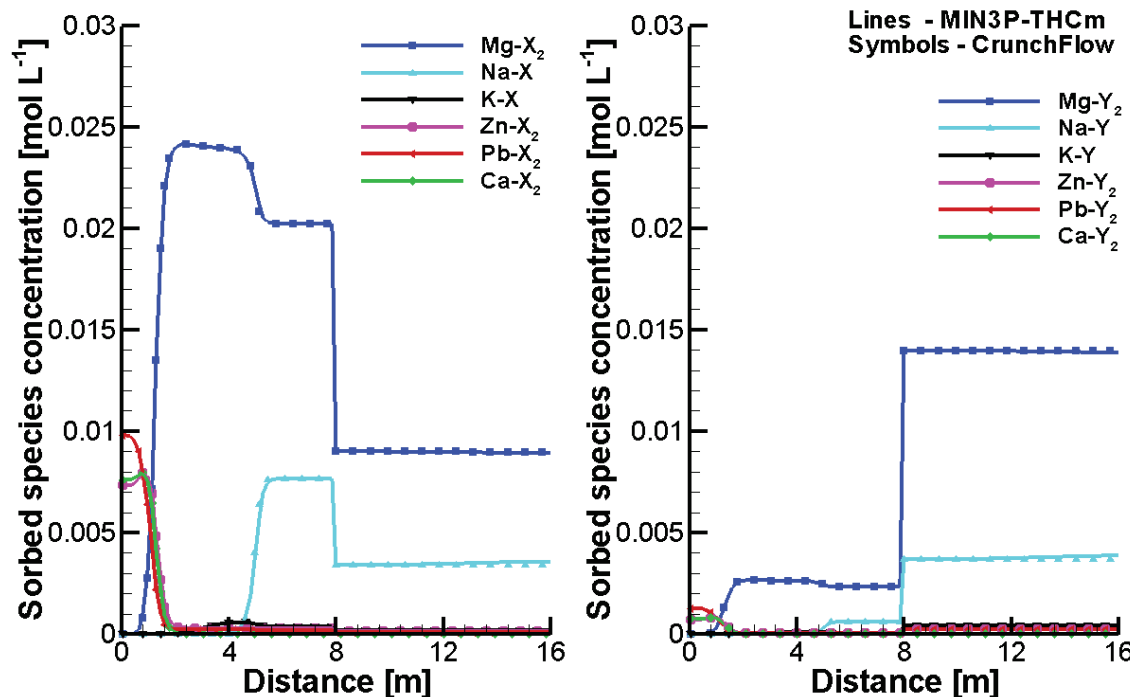


Figure 3: Comparison of Breakthrough Curves at the Outflow Boundary Calculated by MIN3P-THCm (Lines) and CrunchFlow (Symbols): (a) Total Concentrations of Components in the Aqueous Phase, (b) pH, (c) Concentrations of Sorbed Species on Site -X, (d) Concentrations of Sorbed Species on Site -Y

Table 3: Ion Exchange Reactions Used in the Simulation

	Cation exchange reactions	Selectivity coefficients ($\log K_c$)
1	$2\text{Na-X} + \text{Mg}^{2+} \rightleftharpoons \text{Mg-X}_2 + 2\text{Na}^+$	0.6
2	$\text{Na-X} + \text{K}^+ \rightleftharpoons \text{K-X} + \text{Na}^+$	0.7
3	$2\text{Na-X} + \text{Zn}^{2+} \rightleftharpoons \text{Zn-X}_2 + 2\text{Na}^+$	0.8
4	$2\text{Na-X} + \text{Pb}^{2+} \rightleftharpoons \text{Pb-X}_2 + 2\text{Na}^+$	1.0458
5	$2\text{Na-X} + \text{Ca}^{2+} \rightleftharpoons \text{Ca-X}_2 + 2\text{Na}^+$	0.8
6	$\text{Na-X} + \text{Na}^+ \rightleftharpoons \text{Na-X} + \text{Na}^+$	0.0
7	$2\text{Na-Y} + \text{Mg}^{2+} \rightleftharpoons \text{Mg-Y}_2 + 2\text{Na}^+$	0.9
8	$\text{Na-Y} + \text{K}^+ \rightleftharpoons \text{K-Y} + \text{Na}^+$	1.05
9	$2\text{Na-Y} + \text{Zn}^{2+} \rightleftharpoons \text{Zn-Y}_2 + 2\text{Na}^+$	1.2
10	$2\text{Na-Y} + \text{Pb}^{2+} \rightleftharpoons \text{Pb-Y}_2 + 2\text{Na}^+$	1.5687
11	$2\text{Na-Y} + \text{Ca}^{2+} \rightleftharpoons \text{Ca-Y}_2 + 2\text{Na}^+$	1.2
12	$\text{Na-Y} + \text{Na}^+ \rightleftharpoons \text{Na-Y} + \text{Na}^+$	0.0

**Figure 4: Comparison of Sorbed Species Concentration Profiles at 10 Hours Simulated by MIN3P-THCm (Lines) and CrunchFlow (Symbols), Left – Sorbed Species on site –X, Right - Sorbed Species on Site –Y**

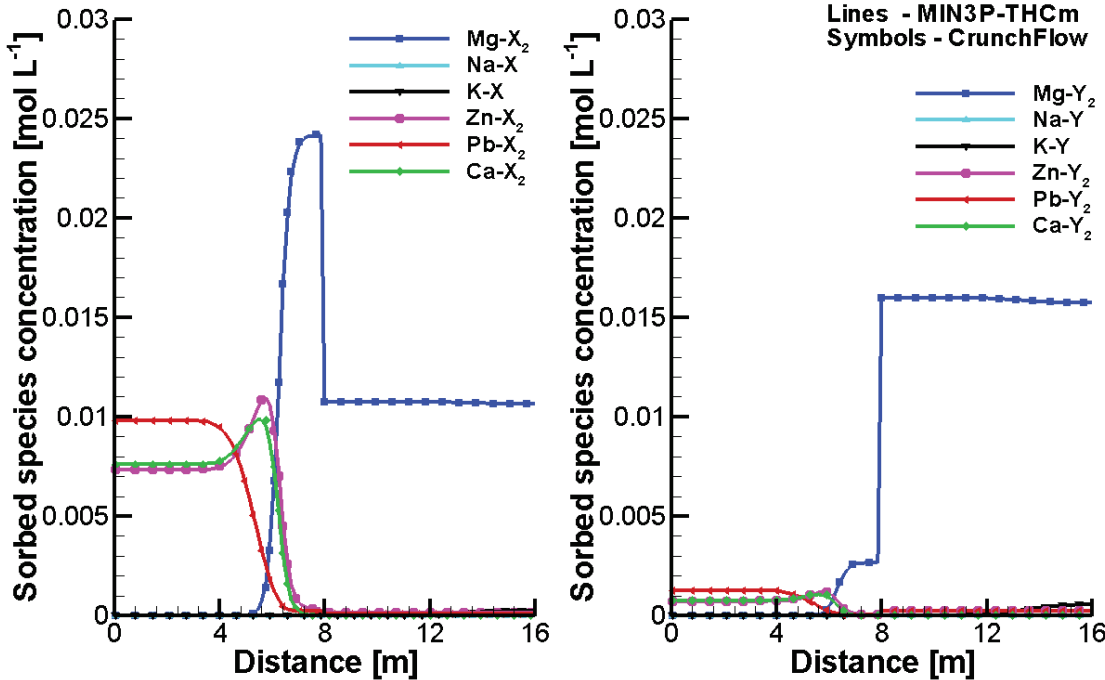


Figure 5: Comparison of Sorbed Species Concentration Profiles at 50 Hours Simulated by MIN3P-THCm (Lines) and CrunchFlow (Symbols), Left – Sorbed Species on Site –X, Right - Sorbed Species on Site –Y

The displacement fronts progress from the inflow boundary towards the right hand side with time (Figure 4, Figure 5). After about 180 hours, the domain has approached an equilibrium condition with Zn^{2+} , Pb^{2+} and Ca^{2+} both in the aqueous phase (Figure 3(a)) and the sorbed species (Figure 3(c) and (d)). At this point in time, the domain is in equilibrium with the inflowing groundwater. The simulated results obtained with MIN3P-THCm are in excellent agreement with the results obtained with CrunchFlow.

4.1.5 Data Location

Input file:

.\Benchmark\benchmarks_new_add\multisite-ionx-V1.0.129\ionx-m-2domains\ionx-2m.dat

Database

.\Benchmark\benchmarks_new_add\multisite-ionx-V1.0.129\database\surfx-ionx-phreeqc1

4.2 MULTICOMPONENT DIFFUSION

The multicomponent diffusion formulation implemented in MIN3P-THCm version 1.0.203 was verified through several benchmarks (Rasouli 2015) by making comparisons to results obtained by CrunchFlow (Steefel 2008) and PHREEQC (Appelo and Wersin 2007; Appelo et al. 2010). One of the benchmarks is selected for inclusion in this report and is described below.

4.2.1 Problem Definition

This benchmark, involving the diffusion of nitric acid into a NaCl solution, is presented here to demonstrate the effect of electromigration and to serve as a verification example for the MCD model.

4.2.2 Model Setup

The electromigration problem was simulated in a 1.0 m long, one-dimensional, horizontal domain, with a dilute NaCl background solution with pH = 6. Nitric acid was allowed to diffuse into the domain from the left hand side boundary. The model was discretized into 100 cells with $\Delta x = 0.01$ m and the simulations were executed for a period of 100 days.

4.2.3 Parameters

The molecular diffusion coefficients (D_0) of all components are summarized in Table 4. The domain is homogeneous with a porosity of 0.25.

Table 4: Selected Model Parameters Used for the Simulation of Nitric Acid Diffusion in NaCl Solution

Transport Parameters	Symbol	Value	Units
Porosity	ϕ	0.25	-
Free aqueous diffusion coefficients (D_0)	$D_0(H^+)$	9.311×10^{-9}	
	$D_0(Na^+)$	1.334×10^{-9}	
	$D_0(Cl^-)$	2.032×10^{-9}	$m^2 s^{-1}$
	$D_0(NO_3^-)$	1.902×10^{-9}	

4.2.4 Results

The concentrations of the ions Na^+ and Cl^- in the solutions at both boundaries are the same as in the initial pore water of the domain (Figure 6 top). After 100 days, however, concentration gradients of both ions Na^+ and Cl^- were established within the domain (Figure 6).

This behavior is caused by the multicomponent diffusion effect. Because H^+ has a larger diffusion coefficient than the anion NO_3^- (Table 4), a local charge imbalance is generated within the domain that in turn provides the driving force for the diffusion of Na^+ and Cl^- to maintain local charge balance in the solution. Na^+ is expelled from the domain, while Cl^- is drawn into the domain to maintain charge balance. The concentration difference of H^+ and NO_3^- reaches a maximum at a position of $x=0.3$ m after 100 days, coinciding with the location where the concentrations of Na^+ and Cl^- differ the most (Figure 6). Excellent agreement is obtained between MIN3P-THCm, CrunchFlow and PHREEQC.

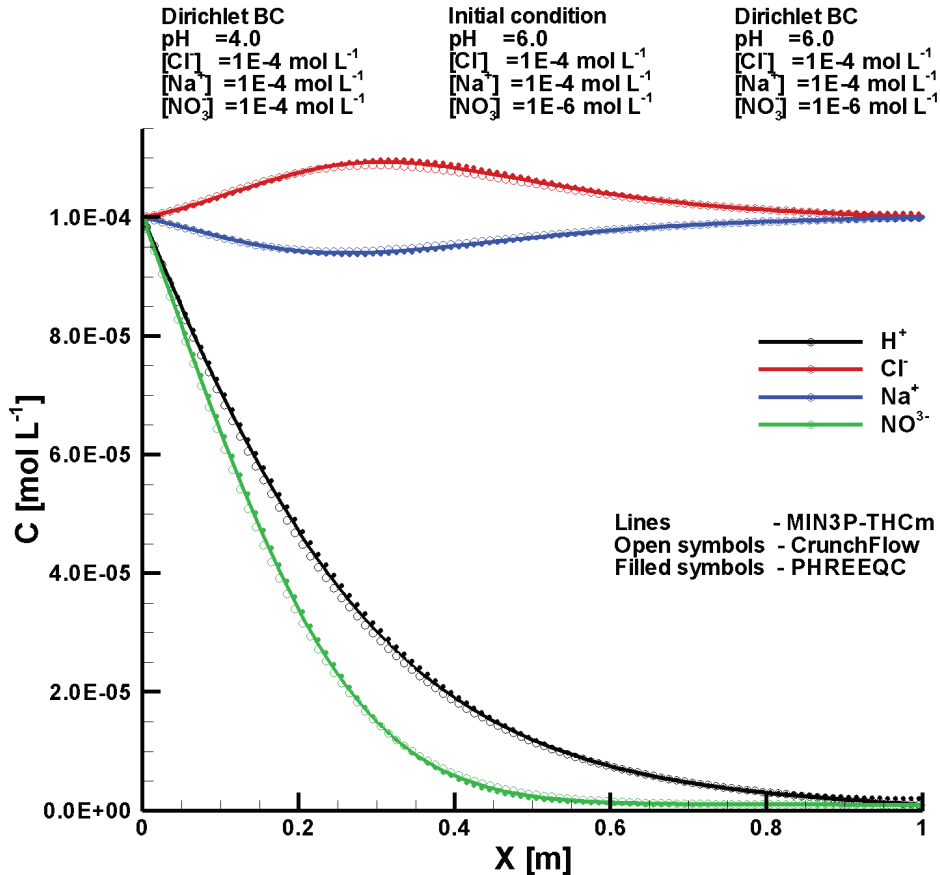


Figure 6: Comparison of Simulated Concentration Profiles Obtained from MIN3P-THCm (Lines), CrunchFlow (Open Symbols) and PHREEQC (Filled Symbols) at 100 Days

4.2.5 File Location

Input file:

.\Benchmark\benchmarks_standard\reactran\MCD-2\min3p\test.dat

Databases:

.\Benchmark\benchmarks_standard\reactran\MCD-2\min3p\database\

4.3 MULTICOMPONENT DIFFUSION IN RADIAL COORDINATES

This benchmark is designed to verify the multicomponent diffusion (MCD) model in radial coordinates through code intercomparison with CrunchFlow.

4.3.1 Problem Definition

The problem is based on the benchmark described in section 4.2; however, the problem is solved using a radial coordinate system with modified boundary conditions.

4.3.2 Model Setup

The electromigration problem was simulated for a one-dimensional system with a radial extent of 1.0 m. Nitric acid was allowed to diffuse into the domain from the outer boundary (on the right) towards the center of the domain. The initial concentrations of Na^+ and Cl^- within the domain are $1.0 \times 10^{-4} \text{ mol L}^{-1}$, which is the same in the solution at the right boundary. The initial pH value within the domain is 6.0, while the pH value at the right boundary is 4.0. The initial concentration of the nitric acid within the domain is $1.0 \times 10^{-6} \text{ mol L}^{-1}$, which is two orders of magnitude lower than that at the right boundary. A zero-flux boundary is assumed at the left side of the domain. The model was discretized into 100 cells with $\Delta r = 0.01 \text{ m}$ and the simulations were executed for a period of 100 days.

4.3.3 Results

Figure 7 compares the species concentration profiles at 100 days. The concentration profiles of Na^+ and Cl^- within the domain show different concentration gradients, although both species were initially present at the same concentration throughout the domain (Figure 7). This behavior is caused by the multicomponent diffusion effect. The concentration difference of H^+ and NO_3^- reaches a maximum at a position of $r = 0.7 \text{ m}$ after 100 days, coinciding with the location where the concentrations of Na^+ and Cl^- differ the most (Figure 7). Excellent agreement is obtained between MIN3P-THCm and CrunchFlow.

4.3.4 File Location

Input file:

`.\Benchmark\benchmarks_standard\reactran\MCD-2-r\min3p\mcd-rc.dat`

Databases:

`.\Benchmark\benchmarks_standard\reactran\MCD-2-r\min3p\database\`

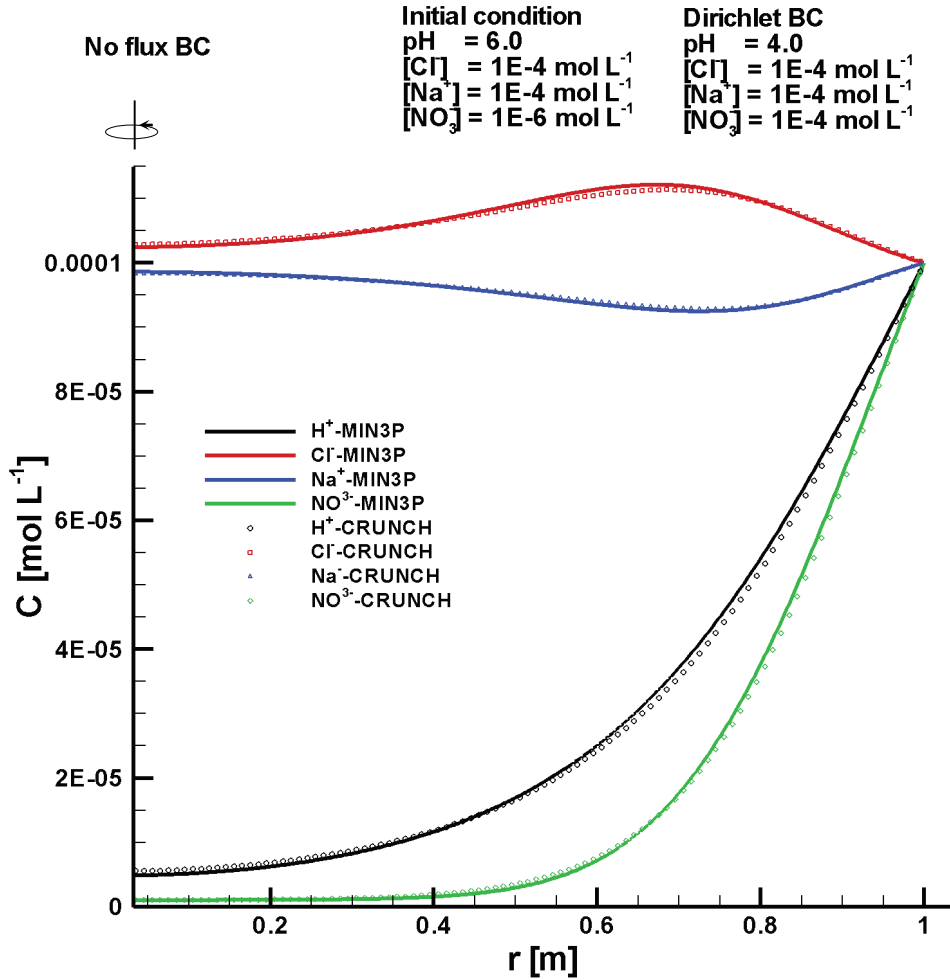


Figure 7: Comparison of Simulated Concentration Profiles Obtained from MIN3P-THCm (Lines) and CrunchFlow (Symbols) at 100 Days

4.4 HYBRID MULTICOMPONENT DIFFUSION IN RADIAL COORDINATES

4.4.1 Problem Definition

This illustrative example demonstrates the use of the hybrid multicomponent diffusion model in radial coordinates. The example is based on previous simulations of the DR-A in situ borehole diffusion experiment at the Mont Terri Underground Rock Laboratory (Xie et al. 2014). The experiment included the injection of tracers into a borehole and the measurement of the tracer concentration time curves in the solution circulating through the borehole circulation chamber (Fierz and Rösli 2012). To ensure pure diffusion conditions, the pore water pressure was automatically adjusted and the flow rate was monitored until no net flux was observed before the tracer diffusion experiment began (Fierz and Rösli 2012).

4.4.2 Model Setup

The diffusion of the tracers from the injection solution into the surrounding media can be represented by a one-dimensional axial symmetric model as shown in Figure 8. The problem was simulated in a one-dimensional domain, extending 61.5 cm in the radial direction, and includes the borehole, a filter, an open gap, and Opalinus Clay (OPA) as the receiving geological formation. The domain was discretized into 165 control volumes. The final simulation time was 189 days.

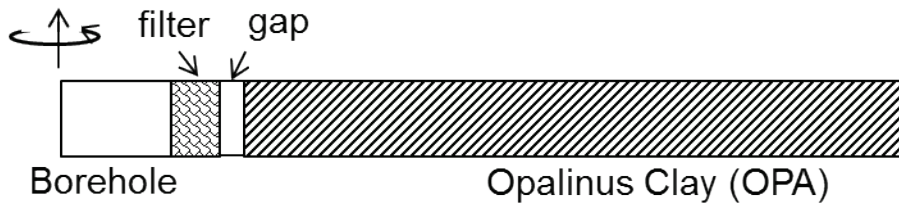


Figure 8: Schematic Diagram of the Simulation Domain Representing the Experimental Set-up Including the Borehole (Radius= 3.1 cm) that Contains the Tracers in Solution, Filter (4 mm in Thickness), Gap (3 mm in Thickness), and OPA up to A Radius of 61.5 cm. A Radial Coordinate System Was Used for the Simulations.

4.4.3 Selected Experimental Data

A mixture of tracers including HTO, $^{85}\text{Sr}^{2+}$, I⁻ and Br⁻ was added to a tank with synthetic Opalinus pore water (Table 5) and injected into the test chamber through the circulation system. The initial chemical composition of the pore water in OPA was specified as listed in Table 6. The concentrations of all tracers were measured at designated times. The measured results, after making any necessary corrections for decay, are listed in Table 7.

Table 5: Composition of the Synthetic OPA Pore Water Used in the DR-A Diffusion and Sorption Experiments - Phase I (Calculated Based on NAGRA (2012))

Element	Total concentration [mol L ⁻¹]
Na ⁺	2.56×10^{-01}
K ⁺	1.80×10^{-03}
Mg ²⁺	1.85×10^{-02}
Ca ²⁺	2.12×10^{-02}
Sr ²⁺	5.85×10^{-04}
Cl ⁻	3.13×10^{-01}
SO ₄ ²⁻	1.45×10^{-02}
TOC	1.42×10^{-03}
pH	7.56

Table 6: Composition of the Initial OPA Pore Water Used in the Simulation of the DR-A Diffusion and Sorption Experiments - Phase I (Based on Van Loon et al. 2003)

Element	Total concentration [mol L ⁻¹]
Na ⁺	2.40×10 ⁻⁰¹
K ⁺	1.60×10 ⁻⁰³
Mg ²⁺	1.70×10 ⁻⁰²
Ca ²⁺	2.60×10 ⁻⁰²
Sr ²⁺	5.10×10 ⁻⁰⁴
Cl ⁻	3.00×10 ⁻⁰¹
SO ₄ ²⁻	1.40×10 ⁻⁰²
CO ₃ ²⁻ /HCO ₃ ⁻	4.76×10 ⁻⁰⁴
pH	7.6
Sum cations	0.328 eq L ⁻¹
Sum anions	0.328 eq L ⁻¹
Ionic strength	0.39 mol L ⁻¹

Table 7: Selected Measured Tracer Concentrations [mol L⁻¹] during the DR-A In-situ Diffusion Experiment - Phase I (Calculated Based on NAGRA (2012))

Time [days]	HTO [mol L ⁻¹]	⁸⁵ Sr ²⁺ [mol L ⁻¹]	I ⁻ [mol L ⁻¹]	Br ⁻ [mol L ⁻¹]
0.0	1.20×10 ⁻¹⁰	5.88×10 ⁻¹⁴	1.11×10 ⁻⁰²	1.11×10 ⁻⁰²
0.1	1.11×10 ⁻¹⁰	5.81×10 ⁻¹⁴	1.04×10 ⁻⁰²	1.05×10 ⁻⁰²
0.3	1.08×10 ⁻¹⁰	5.27×10 ⁻¹⁴	1.00×10 ⁻⁰²	1.01×10 ⁻⁰²
0.9	1.05×10 ⁻¹⁰	5.19×10 ⁻¹⁴	1.00×10 ⁻⁰²	1.02×10 ⁻⁰²
1.2	1.05×10 ⁻¹⁰	5.00×10 ⁻¹⁴	9.95×10 ⁻⁰³	1.00×10 ⁻⁰²
2.0	1.06×10 ⁻¹⁰	4.95×10 ⁻¹⁴	9.94×10 ⁻⁰³	1.00×10 ⁻⁰²
3.0	1.04×10 ⁻¹⁰	4.92×10 ⁻¹⁴	9.81×10 ⁻⁰³	9.98×10 ⁻⁰³
4.0	1.04×10 ⁻¹⁰	4.81×10 ⁻¹⁴	9.88×10 ⁻⁰³	9.95×10 ⁻⁰³
5.0	1.03×10 ⁻¹⁰	4.68×10 ⁻¹⁴	9.79×10 ⁻⁰³	9.90×10 ⁻⁰³
7.0	1.01×10 ⁻¹⁰	4.70×10 ⁻¹⁴	9.77×10 ⁻⁰³	9.87×10 ⁻⁰³
10.0	9.92×10 ⁻¹¹	4.40×10 ⁻¹⁴	9.63×10 ⁻⁰³	9.71×10 ⁻⁰³
14.0	9.77×10 ⁻¹¹	4.25×10 ⁻¹⁴	9.58×10 ⁻⁰³	9.66×10 ⁻⁰³
21.0	9.61×10 ⁻¹¹	4.01×10 ⁻¹⁴	9.56×10 ⁻⁰³	9.65×10 ⁻⁰³
29.0	9.49×10 ⁻¹¹	3.76×10 ⁻¹⁴	9.46×10 ⁻⁰³	9.55×10 ⁻⁰³
43.0	9.28×10 ⁻¹¹	3.49×10 ⁻¹⁴	9.43×10 ⁻⁰³	9.50×10 ⁻⁰³
63.0	8.92×10 ⁻¹¹	3.14×10 ⁻¹⁴	9.19×10 ⁻⁰³	9.24×10 ⁻⁰³
85.4	-	2.93×10 ⁻¹⁴	9.07×10 ⁻⁰³	9.05×10 ⁻⁰³
113.0	8.67×10 ⁻¹¹	2.77×10 ⁻¹⁴	8.87×10 ⁻⁰³	8.94×10 ⁻⁰³
168.8	8.17×10 ⁻¹¹	2.37×10 ⁻¹⁴	8.46×10 ⁻⁰³	8.69×10 ⁻⁰³

- Not measured

4.4.4 Parameters

Key modelling parameters used in the simulations are listed in Table 8.

Table 8: General Parameters for the Circulation Chamber, Filter, Gap and OPA

Parameter	Borehole	Filter	Gap	OPA
Porosity [-]	3.262 ^a	0.45	1.0	0.15
Solid dry bulk density [kg/m ³]	-	-	-	2310.0 ^b

^aborehole capacity ^b Bossart (2013)

The free aqueous diffusion coefficients D_0 listed in Table 9 were used, which were based on the CRC Handbook of Chemistry and Physics (Lide 1994). The effective tortuosity of OPA ($\tau_e = 0.12$) is a fitted parameter based on the measured HTO concentration time curve. Selected effective porosity correction factors ($f_{\phi,j}^c$) and effective tortuosity correction factors ($f_{\tau,j}^c$) for the primary species are listed in Table 9, in which the $f_{\phi,j}^c$ factors for I⁻ and Br⁻ are the measured effective porosity values for I⁻ (0.08) and Br⁻ (0.10) divided by the effective porosity measured for HTO (0.15) (van Loon et al. 2003). The effective porosity correction factors for all secondary species $f_{\phi,j}^x$ are set to 0.667 for all anions and 1.0 for all other species. The effective tortuosity correction factors $f_{\tau,j}^x$ for species except I⁻ and Br⁻ are 1.0. The factor $f_{\tau,j}^x$ for I⁻ and Br⁻ are fitted to match the measured concentration time curves. It should be noted that the effect of aqueous complexation is very limited for this problem, implying that the effect of elemental migration in terms of secondary species is close to negligible. The choice of correction factors for secondary species has therefore only a very small effect on the simulation results.

Table 9: Free Aqueous Phase Diffusion Coefficients (D_0) (Lide 1994), Correction Factors

Species	D_0 [$\times 10^{-9}$ m ² s ⁻¹]	$f_{\phi,j}^c$	$f_{\tau,j}^c$	Species	D_0 [$\times 10^{-9}$ m ² s ⁻¹]	$f_{\phi,j}^c$	$f_{\tau,j}^c$
H ⁺	9.311	1.0	1.0	SO ₄ ²⁻	1.065	0.667	1.0
Na ⁺	1.334	1.0	1.0	CO ₃ ²⁻	0.923	0.667	1.0
K ⁺	1.957	1.0	1.0	I ⁻	2.045	0.667	0.55
Mg ²⁺	0.706	1.0	1.0	Br ⁻	2.08	0.533	0.38
Ca ²⁺	0.792	1.0	1.0	HTO	2.23#	1.0	1.0
⁸⁵ Sr ²⁺	0.791	1.0	2.8	Cl ⁻	2.032	0.667	1.0

from O'Reilly and Peterson (1971)

The linear sorption coefficient (K_d) for the tracer ⁸⁵Sr²⁺ was set to 1.0 kg L⁻¹ (Wersin et al. 2008).

4.4.5 Results

Simulated results show that all tracers diffuse through the filter, gap and into the Opalinus Clay. After 189 days, the fronts of all tracers have migrated less than 0.3 m into the clay (Figure 9(d)). The uncharged species HTO diffuses the fastest, while other tracers are retarded through anion

exclusion (I^- and Br^-) or sorption ($^{85}Sr^{2+}$). Simulated concentration time curves of tracers show very good agreement to the measured data (Figure 9(a)-(c)).

4.4.6 File Location

Input file:

`\Benchmark\ benchmarks_new_add\hMCD-V1.0.203\hmcd.dat`

Databases:

`\Benchmark\ benchmarks_new_add\hMCD-V1.0.203\database\`

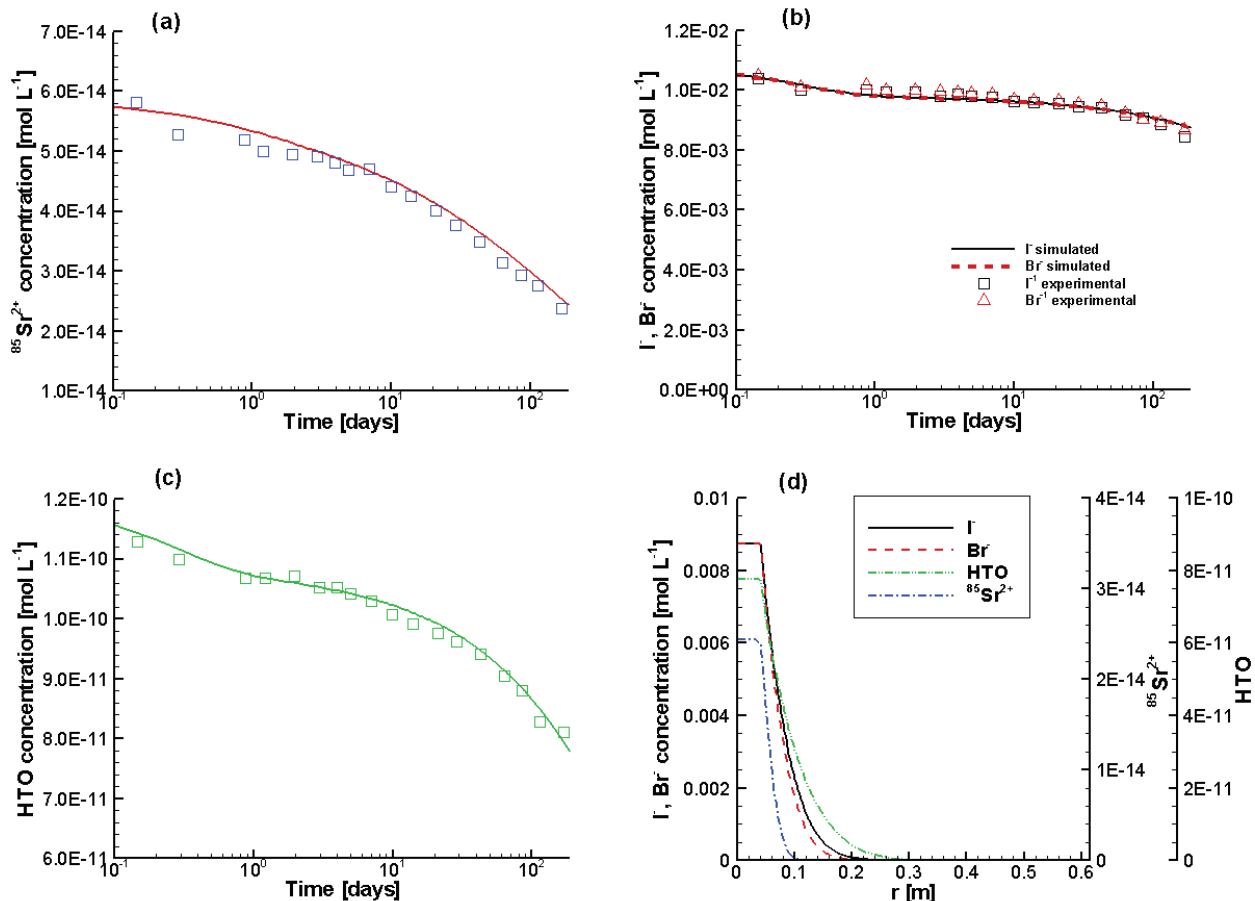


Figure 9: Comparison of Experimental (Symbols) and Simulated (Lines) Concentration Curves of Tracers $^{85}Sr^{2+}$ (a), I^- and Br^- (b), and HTO (c); and the Concentration Profiles of Tracers at 189 Days (d)

5. CONCLUSIONS

Several code enhancements have been implemented into the reactive transport simulator MIN3P-THCm to improve its capabilities for simulation of diffusion dominated geochemical processes. The multisite ion exchange (MIE) model allows for simulation of cation exchange processes on clay minerals (e.g. illite) including different types of exchange sites. The multicomponent diffusion (MCD) model enables MIN3P-THCm to simulate diffusion processes in complex geochemical systems including a mixture of cations and anions that diffuse at different rates (i.e., due to species-dependent diffusion coefficients D_0), but still maintains local charge balance within the domain by accounting for electromigration. An extension of the MCD model led to the development of the hybrid multicomponent diffusion (hMCD) model, which provides an approach to simulate species-dependent diffusion in low permeability media by accounting for anion exclusion, surface and interlayer diffusion in an empirical manner. Both versions of the MCD models were implemented to allow simulations in Cartesian and radial/cylindrical coordinates. The theoretical background, the governing equations, information on code implementation, updates to the user guide for the new code modules, and verification examples for each model have been provided. Model verification was performed through intercomparison with the codes CrunchFlow and PHREEQC, showing favorable agreement for all cases presented. The code enhancements are useful for simulating reactive transport in engineered barrier systems and in low permeability host rocks considered for deep geological repositories.

ACKNOWLEDGEMENTS

This study was funded by the Mont Terri Consortium, Switzerland, and the Nuclear Waste Management Organization (NWMO), Ontario, Canada. Valuable discussions with several colleagues – including Thomas Gimmi (PSI and University of Bern), Olivier Leupin (NAGRA), Josep Soler (IDAEA-CSIC), and especially Tammy (Tianxiao) Yang (NWMO) and Monique Hobbs (NWMO) – have helped to improve this report.

REFERENCES

- Appelo, C.A.J. and D. Postma. 2003. Geochemistry, Groundwater and Pollution, A.A. Balkema, Rotterdam, Netherlands.
- Appelo, C.A.J. and P. Wersin. 2007. Multicomponent diffusion modeling in clay systems with application to the diffusion of tritium, iodide and sodium in Opalinus Clay. *Environmental Science & Technology*, 41, 5002-5007.
- Appelo, C.A.J., A. Vinsot, S. Mettler and S. Wechner. 2008. Obtaining the porewater composition of a clay rock by modelling the in- and out-diffusion of anions and cations from an in-situ experiment. *Journal of Contaminant Hydrology*, 101, 67-76.
- Appelo, C.A.J., L.R. Van Loon and P. Wersin. 2010. Multicomponent diffusion of a suite of tracers (HTO, Cl, Br, I, Na, Sr, Cs) in a single sample of Opalinus Clay. *Geochimica et Cosmochimica Acta*, 74, 1201-1219.
- Bea Jofre, S.A., K.U. Mayer and K.T.B. MacQuarrie. 2011. Modelling Reactive Transport in Sedimentary Rock Environments - Phase II MIN3P code enhancements and illustrative simulations for a glaciation scenario. Nuclear Waste Management Organization Technical Report NWMO TR-2011-13, Toronto, Canada.
- Bea, S. A., K.U. Mayer and K.T.B. MacQuarrie. 2015. Reactive transport and thermo-hydro-mechanical coupling in deep sedimentary basins affected by glaciation cycles: model development, verification and illustrative example, *Geofluids* (accepted July 2015).
- Bea, S.; S. Wilson, K. U. Mayer, G. Dipple, I. Power and P. Gamazo. 2012. Reactive transport modeling of natural carbon sequestration in ultramafic mine tailings. *Vadose Zone Journal*, 11(2), 1-17
- Bear, J. 1972. Dynamics of fluids in porous media, Elsevier Science, New York.
- Bolt, G.H., M.E. Summer and A. Kamphorst. 1963. A study of the equilibrium between three categories of potassium in an illitic soil. *Soil Science Society of America, Proceedings* 27, 294-299.
- Bossart, P. 2013. Characteristics of the Opalinus Clay at Mont Terri, <http://www.mont-terri.ch/>.
- Bourg, I.C., A.C.M. Bourg and G. Sposito. 2003. Modeling diffusion and adsorption in compacted bentonite: a critical review. *Journal of Contaminant Hydrology*, 61, 293-302.
- Bradbury, M. H. and B. Baeyens. 2000. A generalized sorption model for the concentration dependent uptake of caesium by argillaceous rocks. *Journal of Contaminant Hydrology*, 42, 141-163.
- Bradbury, M. H. and B. Baeyens. 2011. Predictive sorption modelling of Ni(II), Co(II), Eu(III), Th(IV) and U(VI) on MX-80 bentonite and Opalinus Clay: A “bottom-up” approach. *Applied Clay Science*, 52, 27-33.
- Brouwer, E., B. Baeyens, A. Maes and A. Cremers. 1983. Cesium and rubidium ion equilibria in illite clay. *Journal of Physical Chemistry*, 87, 1213-1219.

- Chang, H., W. Um, K. Rod, R.J. Serne, A. Thompson, N. Perdrial and J. Chorover. 2011. Strontium and cesium release mechanisms during unsaturated flow through waste-weathered Hanford sediments. *Environmental Science & Technology*, 45, 8313-8320. doi:DOI: 10.1021/es2010368.
- Fierz, T. and U. Rösli. 2012. DR-A Experiment: Instrumentation of BDR-A3 and tracer injection, TECHNICAL NOTE 2011-21, Solexperts AG, Switzerland.
- Galindez, J.M., C.I. Steefel and U. Maeder. 2011. Continuum model for diffusive transport in the electrical double layer and clay interlamellæ. Proceedings at the Goldschmidt 2011 Conference, Prague, Czech Republic, August 14-19, 2011.
- Giambalvo, E.R., C.I. Steefel, A.T. Fisher, N.D. Rosenberg and C.G. Wheat. 2002. Effect of fluid-sediment reaction on hydrothermal fluxes of major elements, eastern flank of the Juan de Fuca Ridge. *Geochimica et Cosmochimica Acta*, 66 (10), 1739–1757.
- Henderson, T., K.U. Mayer, B. Parker and T. Al. 2009. Three-dimensional density-dependent flow and multicomponent reactive transport modeling of chlorinated solvent oxidation by potassium permanganate. *Journal of Contaminant Hydrology*, 106, 195-21.
- Istok, J.D. 1989. Groundwater modeling by the finite element method – (Water resources monograph 13), American Geophysical Union, Washington DC.
- Lapalla, E. G., R.W. Healy and E.P. Weeks. 1987. Documentation of computer program VS2D to solve the equations of fluid flow in variably saturated porous media: U.S. Geological Survey Water-Resources Investigations Report 83-4099.
- Lide, D. 1994. CRC Handbook of chemistry and physics, 74th Edition, 1993-1994, CRC Press/The chemical Rubber Co., Boca Raton, FL. U.S.A.
- Mayer, K.U. 1999. A numerical model for multicomponent reactive transport in variably-saturated porous media, PH.D. – thesis, Department of Earthe Sciences, University of Waterloo, Waterloo, Ontario, Canada.
- Mayer, K.U., E.O. Frind and D.W. Blowes. 2002. Multicomponent reactive transport modeling in variably saturated porous media using a generalized formulation for kinetically controlled reactions. *Water Resources Research*, 38, 1174-1195. doi:10.1029/2001WR000862
- Mayer, K.U. and K. T. B. MacQuarrie. 2010. Solution of the MoMaS reactive transport benchmark with MIN3P - Model formulation and simulation results, *Computers & Geosciences*, 14, 405-419, doi:10.1007/s10596-009-9158-6
- Mayer, K. U., M. Xie, D. Su and K.T.B. MacQuarrie. 2015. MIN3P-THCm - A Three-dimensional Numerical Model for Multicomponent Reactive Transport in Variably Saturated Porous Media, User Guide (unpublished).
- NAGRA, 2012. Mont Terri DR-A field diffusion experiment results (unpublished).
- O'Reilly, D.E. and E.M. Peterson. 1971. Self-Diffusion Coefficients and Rotational Correlation Times in Polar Liquids. II, *The Journal of Chemical Physics*, 55, 2155-2164.

- Parkhurst, D.L. and C.A.J. Appelo. 1999. User's guide to PHREEQ C (Version 2) – a computer program for speciation, batch-reaction, one-dimensional transport and inverse geochemical calculations, Water-Resources Investigations, Report 99-4259, Denver, Co, USA, p. 312.
- Rasouli, P. 2015. The role of multicomponent diffusion and electrochemical migration for reactive transport in porous media, PhD-thesis, University of British Columbia, in progress.
- Shackelford, C.D. and S.M. Moore. 2013. Fickian diffusion of radionuclides for engineered containment barriers: Diffusion coefficients, porosities, and complicating issues. *Engineering Geology*, 152(1):133–147, DOI: 10.1016/j.enggeo.2012.10.014.
- Spiessl, S.M., K.T.B. MacQuarrie and K.U. Mayer 2008. Identification of key parameters controlling dissolved oxygen migration and attenuation in fractured crystalline rocks. *Journal of Contaminant Hydrology*, 95, 141–153.
- Steefel C.I., S. Carroll, P. Zhao and S. Roberts. 2003. Cesium migration in Hanford sediment: a multisite cation exchange model based on laboratory transport experiments. *Journal of Contaminant Hydrology*, 67(1-4), 219-46.
- Steefel C.I. 2008. CrunchFlow. Software for Modeling Multicomponent Reactive Flow and Transport. Lawrence Berkeley National Laboratory, Berkeley, CA, USA.
- Steefel, C.I., D.J. DePaolo and P.C. Lichtner. 2005. Reactive transport modeling: An essential tool and a new research approach for the Earth sciences. *Earth and Planetary Science Letters*, 240, 539– 558.
- Steefel, C.I., C.A.J. Appelo, B. Arora, D. Jacques, T. Kalbacher, O. Kolditz, V. Lagneau, P.C. Lichtner, K.U. Mayer, J.C.L. Meeussen, S. Molins, D. Moulton, H. Shao, J. Simunek, N. Spycher, S.B. Yabusaki and G.T. Yeh. 2014. Reactive transport codes for subsurface environmental simulation. *Computational Geosciences* doi:10.1007/s10596-014-9443-x
- Van Loon, L.R., J.M. Soler and M.H. Bradbury. 2003. Diffusion of HTO, ^{36}Cl and ^{125}I in Opalinus Clay samples from Mont Terri – effect of confining pressure. *Journal of Contaminant Hydrology*, 61, 73–83.
- Wersin, P., E. Curti and C.A.J. Appelo. 2004. Modelling bentonite–water interactions at high solid/liquid ratios: swelling and diffuse double layer effects. *Applied Clay Science*, 26(1–4), 249–257.
- Wersin, P., J.M. Soler, L.V. Loon, J. Eikenberg, B. Baeyens, D. Grolimund, T. Gimmi and S. Dewonck. 2008. Diffusion of HTO, Br⁻, I⁻, Cs⁺, 85-Sr²⁺ and 60-Co²⁺ in a clay formation: Results and modelling from an in situ experiment in Opalinus Clay. *Applied Geochemistry*, 23, 678-691.
- Xie, M., P. Rasouli, K. U. Mayer and K. T. B. MacQuarrie. 2014. Reactive Transport Modelling of In-situ Diffusion Experiments for the Mont Terri Project MIN3P-THCm Code Enhancements and Numerical Simulations, Nuclear Waste Management Organization Technical Report NWMO-TR-2014-25. Toronto, Canada.

Zachara, J. M., S. C. Smith, C. Liu, J. P. McKinley, R. J. Serne and P. L. Gassman. 2002.
Sorption of Cs⁺ to micaceous subsurface sediments from the Hanford site, USA.
Geochimica et Cosmochimica Acta, 66, 193-211.